Article

Current Biology

Non-cell-autonomous signaling associated with barley ALOG1 specifies spikelet meristem determinacy

Highlights

- Recessive alleles of barley *ALOG1* (*HvALOG1*) give rise to extra spikelets
- *HvALOG1* is specifically expressed in boundaries and not in reproductive meristems
- *HvALOG1* specifies spikelet meristem determinacy and floral organ development
- ALOG family members may operate jointly to shape inflorescence architecture

Authors

Guojing Jiang, Ravi Koppolu, Twan Rutten, ..., Jochen Kumlehn, Martin Mascher, Thorsten Schnurbusch

Correspondence

schnurbusch@ipk-gatersleben.de

In brief

Jiang et al. show that barley ALOG1 (HvALOG1) prevents the production of extra spikelets. HvALOG1 has a boundary-specific expression pattern that excludes reproductive meristems and is associated with non-cell-autonomous signals to specify spikelet meristem identity. Other ALOG family members may operate jointly to shape inflorescence architecture.

Jiang et al., 2024, Current Biology *34*, 2344–2358
June 3, 2024
https://doi.org/10.1016/j.cub.2024.04.083

CellPress

CellPress
OPEN ACCESS

Current Biology

Article

Non-cell-autonomous signaling associated with barley ALOG1 specifies spikelet meristem determinacy

Guojing Jiang,[1,4] Ravi Koppolu,[1] Twan Rutten,[1] Goetz Hensel,[1] Udda Lundqvist,[2,5] Yudelsy Antonia Tandron Moya,[1] Yongyu Huang,[1] Jeyaraman Rajaraman,[1] Naser Poursarebani,[1] Nicolaus von Wirén,[1] Jochen Kumlehn,[1] Martin Mascher,[1] and Thorsten Schnurbusch[1,3,6,*]

[1]Leibniz Institute of Plant Genetics and Crop Plant Research (IPK) Gatersleben, Corrensstr. 3, 06466 Seeland, Germany
[2]Nordic Genetic Resource Center, SE-23053 Alnarp, Sweden
[3]Faculty of Natural Sciences III, Institute of Agricultural and Nutritional Sciences, Martin Luther University Halle-Wittenberg, 06120 Halle, Germany
[4]Present address: Cell Biology and Plant Biochemistry, University of Regensburg, Universitätsstrasse 31, 93053 Regensburg, Germany
[5]Deceased
[6]Lead contact
*Correspondence: schnurbusch@ipk-gatersleben.de
https://doi.org/10.1016/j.cub.2024.04.083

SUMMARY

Inflorescence architecture and crop productivity are often tightly coupled in our major cereal crops. However, the underlying genetic mechanisms controlling cereal inflorescence development remain poorly understood. Here, we identified recessive alleles of barley (*Hordeum vulgare* L.) *HvALOG1* (*Arabidopsis thaliana LSH1* and *Oryza G1*) that produce non-canonical extra spikelets and fused glumes abaxially to the central spikelet from the upper-mid portion until the tip of the inflorescence. Notably, we found that HvALOG1 exhibits a boundary-specific expression pattern that specifically excludes reproductive meristems, implying the involvement of previously proposed localized signaling centers for branch regulation. Importantly, during early spikelet formation, non-cell-autonomous signals associated with HvALOG1 expression may specify spikelet meristem determinacy, while boundary formation of floret organs appears to be coordinated in a cell-autonomous manner. Moreover, barley ALOG family members synergistically modulate inflorescence morphology, with *HvALOG1* predominantly governing meristem maintenance and floral organ development. We further propose that spatiotemporal redundancies of expressed HvALOG members specifically in the basal inflorescence may be accountable for proper patterning of spikelet formation in mutant plants. Our research offers new perspectives on regulatory signaling roles of ALOG transcription factors during the development of reproductive meristems in cereal inflorescences.

INTRODUCTION

The primary factors defining inflorescence architecture are the duration of inflorescence meristem (IM) activity, the number of initiated meristems, and their spatial arrangement.[1,2] In Triticeae species, such as wheat (*Triticum* ssp.) or barley (*Hordeum vulgare* L.), the IM serves as the initial reproductive meristem that provides cells for the formation and differentiation of distichously arranged axillary meristems, termed spikelet meristems (SMs), which ultimately develop into spikelets, the fundamental reproductive units across grass inflorescences.[3] In wheat, single spikelets are arranged on the inflorescence rachis, while in barley, spikelet triplets originate from the same rachis node.[2] In both wheat and barley, genetic modifications of these canonical spikelet arrangements have been reported that lead to the formation of non-canonical extra spikelets per rachis node, resulting in an increased number of spikelets[4–9] and, ultimately, higher grain yield.[10]

The identity and determinacy of many grass meristems are partially determined by a group of genes expressed specifically at organ boundaries, which can form local signaling centers that regulate adjacent meristem fate and activity in a non-cell-autonomous fashion.[11] The formation of organ boundaries during inflorescence development is a complex process encompassing intercellular signaling, intricate gene regulatory networks, and precisely controlled cell division, expansion, and differentiation.[12,13] Boundary-specific expression of genes is critical for establishing and maintaining organ boundaries, with the synergistic action of these genes regulating diverse cell identities, axillary meristem initiation, and proper development of neighboring organs and tissues.[11,14] In *Arabidopsis*, the canonical mechanisms for organ boundary formation are defined by a regulatory network centered around *CUP-SHAPED COTYLEDON* (*CUC*) genes.[12,14,13] *CUC* genes are expressed in boundary domains between organs and primordia, and the inactivation of any two *CUC* genes leads to the fusion of normally separated adjacent

organs.[15–18] Moreover, two *Arabidopsis thaliana LSH1* and *Oryza G1* (*ALOG*) family members, *ORGAN BOUNDARY1/LIGHT-DEPENDENT SHORT HYPOCOTYL 3* (*OBO1/LSH3*) and *OBO4/LSH4*, function downstream of *CUC1* and are expressed specifically at shoot organ/primordia boundaries, inhibiting boundary cell differentiation.[15,19–21] The ALOG proteins, a plant-specific transcription factor (TF) family, have been implicated as key regulators in light signaling, boundary establishment, floral organ specification, meristem maintenance, and inflorescence development.[19,20,22–35] Intriguingly, ALOG paralogs in tomato can synergistically regulate shoot apical meristem (SAM) maturation, determining flowering transition and compound inflorescence production.[30,31]

Here, we characterized a barley spikelet developmental mutant, *extra floret-a* (*flo.a*), which produced extra spikelets and fused glumes due to the defective establishment of organ boundaries. Through map-based cloning, we identified *Flo.a*, encoding an ALOG protein. We propose that *HvALOG1* and its paralogs modulate SM activity, thereby governing regular inflorescence development in barley.

RESULTS

Characterization of a barley mutant with extra spikelets

In barley, the *Hordeum*-specific triple SM (TSM) originates from the upper axillary spikelet primordium of the double ridge (DR) through bifurcating into three separate SMs that subsequently differentiate into individual spikelets.[2] As the spike develops, new SMs emerge continually and align until the spike reaches its maximum spikelet count,[36] resulting in a gradient of spikelet developmental stages along the length of the spike (Figures S1A and S1B). To investigate the genetic basis of inflorescence development in barley, we examined the spike developmental mutant *flo.a*, characterized by the production of non-canonical extra floral organs abaxial to the central spikelet (CS) (Figures 1A and 1B). The original *flo.a* was generated in the two-rowed barley cultivar Foma through ethyleneimine-induced mutagenesis and subsequently backcrossed five times with cultivar Bowman (BW, wild type in this study) to establish a near-isogenic line (BW-NIL-*flo.a*; referred to here as *flo.a*), displaying a spike phenotype identical to the ancestral mutant.[37]

The *flo.a* mutant was initially documented to exhibit extra floral bracts growing from the same rachis node as the original spikelet triplets, particularly from the CS region.[37] However, our phenotypic examinations discerned a consistent emergence of an extra pair of glumes accompanying these additional floral bracts. Given that a pair of glumes is diagnostic of an established spikelet identity, we infer that all these observed extra structures are spikelet derived (Figures 1A–1C). It was common for these extra spikelets to not fully develop into grains, mirroring the limited development seen in lateral spikelets (LSs) of two-rowed barley (Figure 1D). The *flo.a* mutant produced not only completely sterile extra spikelets but also other floral structures, such as glumes, paleae, and lemmas, with varying degrees of deformities (Figures S1C–S1I). Notably, besides the extra spikelets, the *flo.a* phenotype featured several pairs of CS glumes that had long awns or were even fused at the base to form broader, leaf-like bracts (Figure 1B). Intriguingly, all the observed defects in *flo.a* were restricted to the upper-middle section of the spike, omitting the basal section, suggesting a spatially regulated impact of the *flo.a* locus on barley spike development (Figures 1A and 1E–1G). Moreover, floret development of LSs was severely inhibited in *flo.a* in both the apical and basal parts of the spike, resulting in significantly smaller LSs compared to BW (Figures S1J–S1L). Subsequent phenotypic analyses revealed that the extra spikelets in *flo.a* formed on the abaxial side of the CS at the rachis node (Figures S1M–S1R and S1T); however, their floret primordia, including stamens, pistil, and ovary, did not continue to develop and eventually degenerated (Figures 2D and S1R). Furthermore, the two glumes of the CS frequently displayed partial fusion close to the base, adjacent to a newly differentiated primordium of unknown identity (Figures S1P, S1Q, and S1T), indicating defects in boundary establishment.

Developmental time course analysis showed that during early inflorescence developmental stages, the differentiated TSMs are comparable between BW and *flo.a* (Figure S1S). The extra SMs were initially detectable at the middle part of the *flo.a* spike from the lemma primordium (LP) stage (Figures 2A1, 2A8, and S1S). These extra SMs often differentiate into floral primordia and generate one to two florets, resulting in an extra spikelet/floret phenotype (Figures 2A3, 2A4, 2A10, 2A11, S1S, and S1T). Moreover, compared with BW, the growth direction of CSs in the upper-mid part of *flo.a* was not directed toward the inflorescence apex but rather skewed or slightly twisted, suggesting perturbed patterning during immature spike growth (Figures 2A3, 2A4, 2A10, and 2A11). Of note, during the awn primordium (AP) stage, differentiation of LS meristems (LSMs) in *flo.a* was inhibited in the apical region of inflorescence (Figures 2A5–2A7 and 2A12–2A14). Yet by the white anther (WA) stage, both BW and *flo.a* exhibited similar maximal spikelet numbers, suggesting that the arrested LSs result from the *flo.a* mutation rather than the programmed spike degeneration process in barley (Figures 2B and S1S).[36,38] Taken together, our results indicate at least two types of developmental problems in the *flo.a* mutant: the compromised SM determinacy and the impacted boundary and identity of the CS glumes.

Perturbed vascular bundle arrangements in rachis nodes

Barley vascular patterning is intimately related to spike form and development.[39] Each spikelet floral organ is characterized by a distinct vascular arrangement, providing a key to understanding their specific roles within the inflorescence architecture. To examine the vascular connectivity of extra spikelets to the rachis node and its consequential impact on the development of spikelet triplets, we performed a three-dimensional (3D) reconstruction of the rachis node bearing extra floral organs in *flo.a* (Figures S2A–S2C). We identified nearly 50 individual vascular bundles belonging to different spikelet organs, such as glume, lemma, palea, and rachis (Figures S2B and S2C). Only two types of extra-formed organs were detected and showed identical vein numbers to those in the lemma (five veins) and glumes (three veins) of normal CS, thereby supporting the identity of the supernumerary organs as either glumes or lemmas (Figure S2C). Interestingly, the extra lemma vascular bundles (*flo.a* lemma, fL1 to fL5) were able to access the nodal complex despite being different from those in regular CS lemmas in their size and

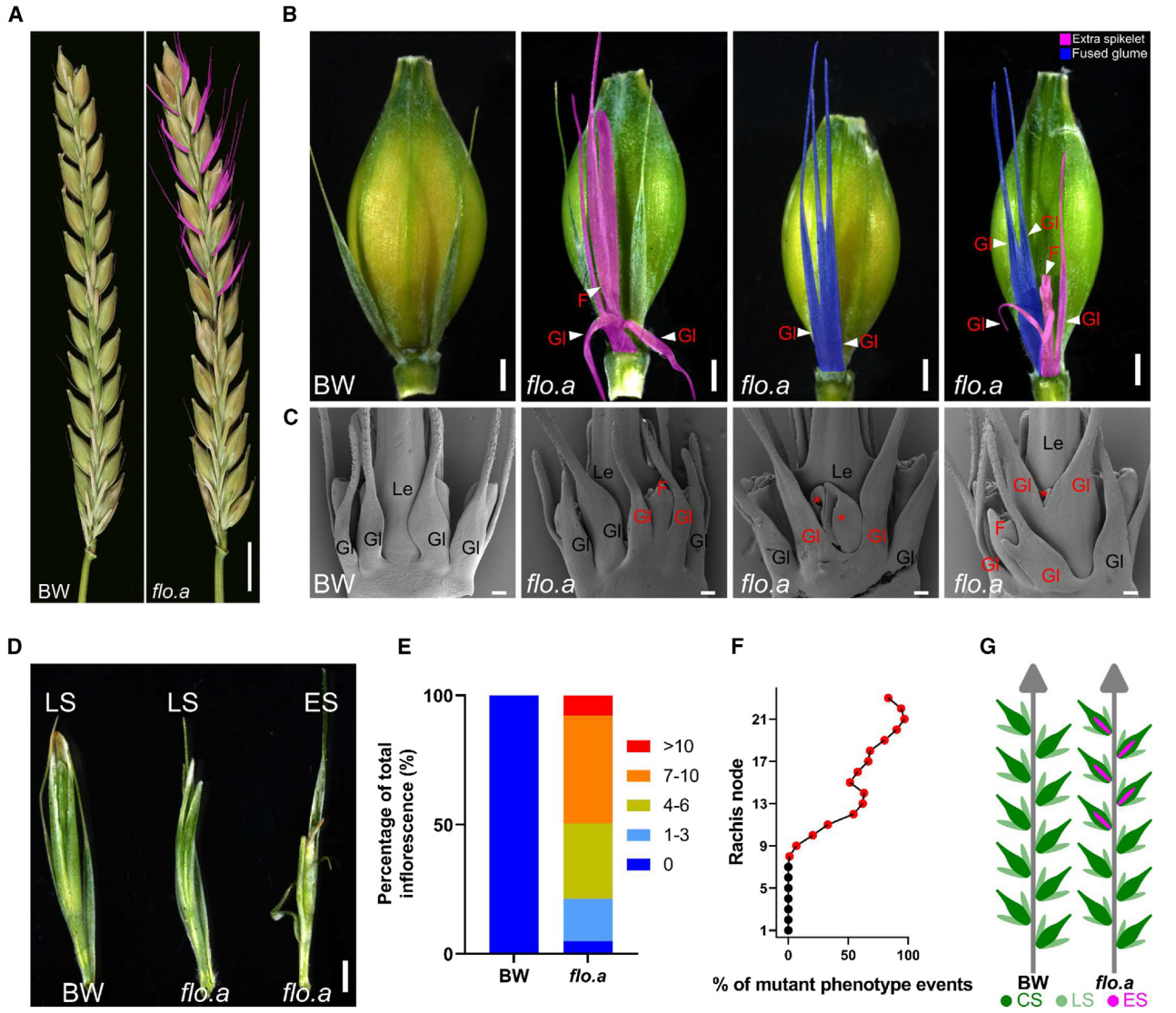

Figure 1. *flo.a* displays paired spikelet and modified inflorescence architecture

(A) The morphology of spike of BW and *flo.a* mutant. The awns of the central spikelet (CS) have been removed. The purple areas represent extra spikelets.

(B) The extra spikelets and fused glume of CS are produced from the abaxial part of CS. The lateral spikelets (LSs) have been removed. The purple and dark blue areas represent extra spikelets and fused glumes, respectively.

(C) Scanning electron microscopy analysis shows extra spikelets and fused glume of CS during early developmental stages in *flo.a* mutant.

(D) Phenotypic comparison of LS and extra spikelet (ES) in BW and *flo.a* mutant.

(E) Quantification of *flo.a* events (extra spikelet and fused glume) in *flo.a* mutant. No *flo.a* event is found in wild type (BW).

(F) Phenotypic distribution of extra spikelet and fused glume under the *flo.a* in the field condition. The black dot and red dot represent the percentage of total extra spikelets and fused glumes in the basal and upper-mid portion part of rachis nodes of *flo.a*, respectively.

(G) Schematic diagram of the phenotype differences between BW and *flo.a*.

The red letters indicate the supernumerary or defective floral organs of the CS. Asterisks indicate the primordia or organs with unknown identity. F, floret; Gl, glume; Le, lemma; Pa, palea; St, stamen.

Scale bar, 1 cm (A); 1 mm (B and D); 100 μm (C).

See also Figures S1 and S7.

absence of strict symmetry patterns (Figures 2C and S2D). Notably, CS lemmas (L4 and L5) were fused near the nodal complex, providing the space for the connection of the vascular bundles of organs from extra spikelets (Figure S2D). Moreover, 3D modeling for glumes revealed that the formation of extra spikelet not only added additional vascular bundles of glumes to the nodal system but also appeared to disturb glumes of the spikelet triplets. Although the central vascular bundles of all six glumes from the spikelet triplet and the two glumes from the extra spikelets merged with the nodal complex, at least five of the 16 lateral vascular bundles were not connected to the peripheral network, particularly the three vascular bundles from the glumes of the CS

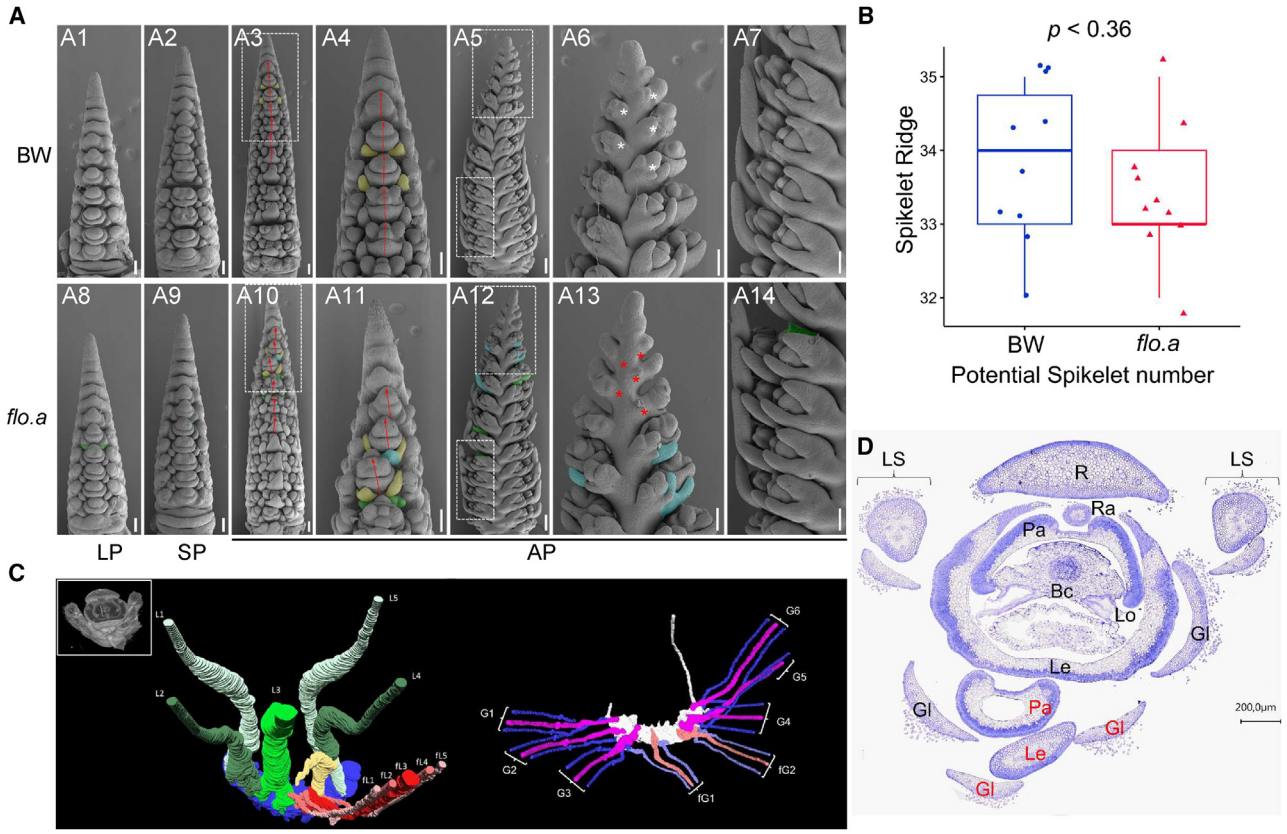

Figure 2. The formation of extra spikelets and fused glumes affects the inflorescence morphology in *flo.a*

(A) Scanning electron micrographs of the immature spike in BW and *flo.a*. The green area represents the extra SM/primordia. The yellow areas represent glume primordia. The blue areas represent newly formed primordium from glume primordia. Asterisks indicate suppressed LS. The red arrows indicate the direction of CS development. LP, lemma primordium; SP, stamen primordium; AP, awn primordium. Scale bar, 100 μm.

(B) Statistical analysis of potential spikelet number in BW and *flo.a*.

(C) 3D reconstruction of vascular bundles for lemma from CS and extra spikelet (left) and for glume from CS, LS, and extra spikelet (right) in *flo.a*. L1 to L5 and fL1 to fL5 represent lemma vascular bundles from CS and extra spikelet, respectively. G1 to G6 and fG1 to fG6 represent glume vascular bundles from CS and extra spikelet, respectively.

(D) Cross-section details of spike phenotype of *flo.a*. The red terms indicate the floral organs of the extra spikelet. BC, basal carpel; Gl, glume; Le, lemma; Lo, lodicule; LS, lateral spikelet; Pa, palea; R, rachis; Ra, rachilla. Scale bar, 200 μm.

See also Figures S1 and S2.

(Figures 2C, S2E, and S2F). This suggests that the formation of additional vascular bundles has a distinct effect on the organ development of spikelet triplets, thereby disrupting the vascular patterning of adjacent organs.

The data presented above indicate that the presence of extra spikelets affects the connection of developing organs to the rachis node, thereby also affecting the development of the CSs. This impact is reciprocal, as the limited space at the nodal complex also constrains the complete development of spikelet quartets, resulting in various shapes of the extra spikelets. This ultimately leads to noticeable differences in spikelet and grain sizes between BW and *flo.a* (Figure S2G).

Map-based cloning and identification of *flo.a* as ALOG family member

To identify the mutations underlying the *flo.a* phenotype, we performed whole-genome sequencing (WGS) of wild type and *flo.a* and found only three introgressions from the original donor line (Foma) within *flo.a* (Figure S3A). Genetic analysis revealed that the phenotypic distribution adhered to a 3:1 ratio (144 wild type to 46 mutant, total 190 individuals in F2) (χ^2 = 0.06, p = 0.80) (Figure S3B), indicating that the *flo.a* phenotype is governed by a singular nuclear monogenic recessive allele.

High-resolution mapping using 3,794 gametes narrowed down the *flo.a* locus to a 12.2 Mbp physical interval on the short arm of chromosome 6H (Figure 3A). We then considered the possibility of chromosomal structural variation within the mapping interval based on WGS data. Sequence analysis showed that one ~477 kb genomic region had drastically lower read coverage in *flo.a* compared to BW and Foma (Figure 3A), suggesting a large genomic deletion in this candidate region. The putatively deleted genomic region contained one high-confidence (HC) and three low-confidence (LC) genes. Further examination of the four annotated genes revealed that the HC gene, *HORVU.MOREX.r2.6HG0469780*, is a member of the ALOG transcriptional regulator family (Figure 3B). RNA sequencing

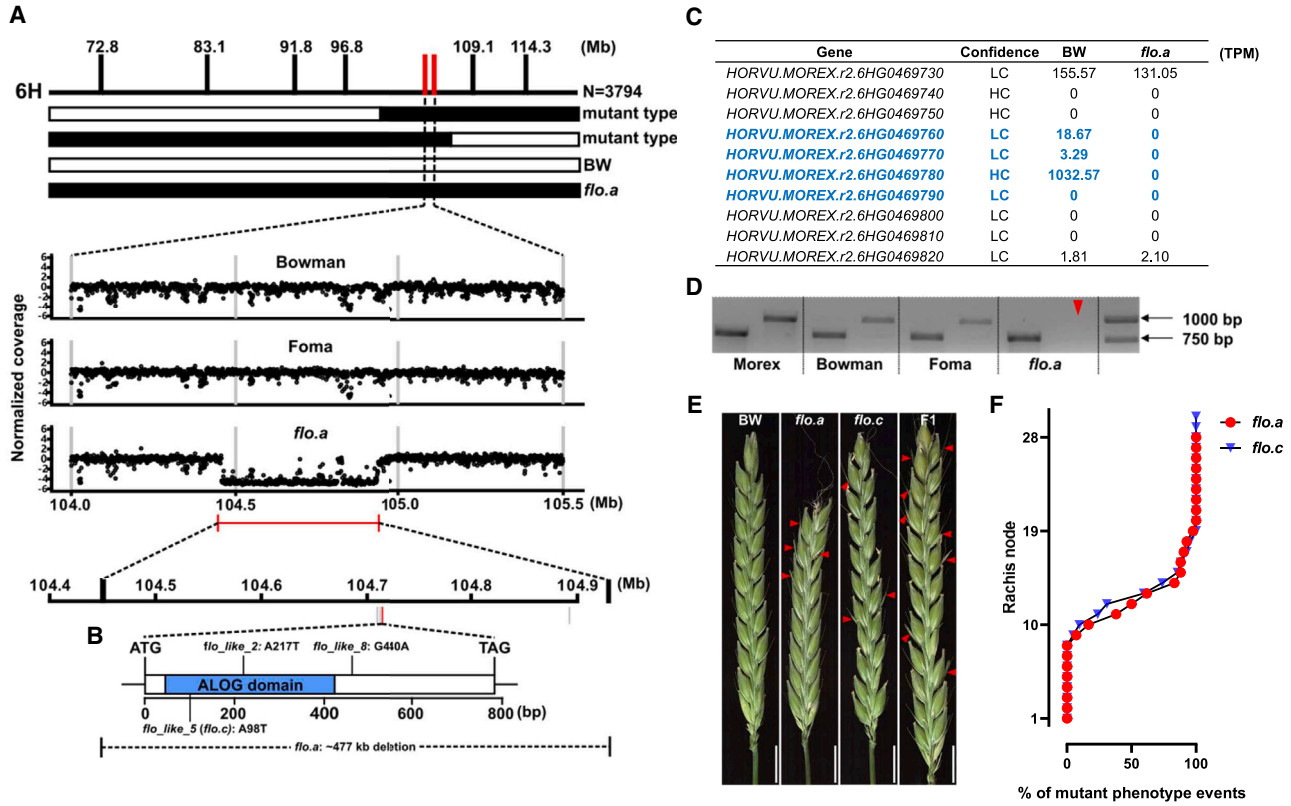

Figure 3. Identification of mutations of *flo.a* locus that promotes the formation of extra spikelet and fused glumes

(A) Map-based cloning of *Flo.a*. *Flo.a* was narrowed down to a 12.2-Mbp interval on the short arm of chromosome 6H. The number of plants used for mapping and the recombinants is indicated. WT, wild type. The genomic region carrying the ~477-kb deleted interval is indicated by the red lines. Normalized coverage of whole-genome sequencing in 1.5-Mbp region between Bowman, Foma, and *flo.a*. The ~477-kb deleted interval is marked by the red line. Gene number in the deleted interval. The red and gray lines indicate high-confidence (HC) and low-confidence (LC) genes, respectively.

(B) *Flo.a* gene model containing one ALOG domain (blue box). The mutation positions in the *Flo.a* gene from four barley mutants showing *flo.a* phenotypes are indicated.

(C) RNA-seq analysis shows that the transcript of genes (blue) located in deleted interval is not detectable in *flo.a*.

(D) PCR amplification by primer pairs covering the *flo.a* candidate (*HORVU.MOREX.r2.6HG0469780*) (right) and flanking gene (*HORVU.MOREX.r2.6HG0469830*) (left) outside of the deletion in Morex, Bowman, Foma, and *flo.a*.

(E) Allelism test between *flo.a* and *flo.c*. The red triangle represents the extra spikelet. Scale bar, 1 cm.

(F) Phenotypic distribution of extra spikelet and fused glume in the *flo.a* and *flo.c* in the greenhouse condition.

See also Figure S3.

(RNA-seq) analysis revealed that transcripts for these four genes were absent in *flo.a*, while *HORVU.MOREX.r2.6HG0469780* displayed high expression in young spike tissues of BW (Figure 3C). PCR amplification confirmed the absence of this gene in *flo.a* (Figure 3D). To validate the underlying candidate gene, we sequenced *HORVU.MOREX.r2.6HG0469780* in two other known *flo* mutants (*flo.b* and *flo.c*), which are in a similar genetic background to *flo.a* and display identical phenotypic defects.[37] *flo.c* was found to carry a non-synonymous mutation in the candidate gene (Figures 3B and S3C). F_1 plants (F_1_*flo.a*/*flo.c*) produced extra spikelets, suggesting that the *flo.c* non-synonymous mutation is allelic to the *flo.a* complete deletion allele (Figures 3E and 3F). Additionally, we collected a set of nine *flo-like* mutants from different genetic backgrounds that display extra spikelets in the upper-mid part of the spike, similar to *flo.a* (Figure S3D). Sanger sequencing of these mutants revealed that three of them, i.e., *flo_like_2*, *flo_like_5* (identical to *flo.c* allele), and *flo_like_8*, carried amino acid substitutions or premature stop codons, resulting in protein truncation (Figures 3B and S3C). These results strongly support that *HORVU.MOREX.r2.6HG0469780* is the causative gene for the *flo.a* phenotype.

HORVU.MOREX.r2.6HG0469780 encodes for a plant-specific TF containing an ALOG domain, which originates from the XerC/D-like recombinases (Figure S3E).[40] We designated this gene as *HvALOG1* because members of this family have not been reported in barley so far. The barley genome contains 10 ALOG genes (*HvALOG1* to *HvALOG10*) (Figures S3F and S3G). Protein alignment analysis in barley revealed that these 10 ALOG family members can be divided into three clades (Figure S3G). Phylogenetic analysis of ALOG proteins across grass and eudicot species revealed that 220 ALOG proteins can be distinctly classified into subgroups corresponding to these two major plant lineages (Figure S3F), consistent with previous studies suggesting that ALOG genes have undergone several independent gene

duplication events across diverse plant lineages.[41,42] ALOG proteins identified across various plant species have been observed to possess similar roles in regulating inflorescence development,[23,29–31,35] suggesting that they likely retained conserved functions in regulating plant reproductive growth. However, the function of HvALOG1 orthologs in grasses has not been identified. We retrieved a total of 10 HvALOG1 orthologs from seven grass species and found the ALOG domain to be highly conserved, especially within the Triticeae (wheat, barley, and rye), with only three amino acid differences (Figure S3E). This suggests that HvALOG1 is likely to perform a conserved function in grasses.

Temporal and spatial expression pattern of *HvALOG1*

To understand the potential role of *HvALOG1* during spikelet formation, we analyzed its transcript and protein expression patterns during inflorescence development. Quantitative real-time PCR showed that *HvALOG1* had the highest expression level in spike tissues at the DR stage with a gradual expression decline in the subsequent developmental stages (Figure 4A). *HvALOG1* was barely detectable in vegetative organs (flag leaves and leaf sheath) (Figure 4A). mRNA *in situ* hybridizations using developing spikes of BW revealed that *HvALOG1* mRNA signal accumulation was initially detected in the leaf ridge (LR) primordia, but not in spikelet ridge primordia (Figures 4B–4E and 4I). At LP stage, *HvALOG1* showed expression signals in primordia of leaf-like floral organs, such as glume, lemma, and palea (Figures 4F and 4G). Later at the AP stage, expression was specifically localized to the base of floret organs (Figures 4H–4K). Intriguingly, all reproductive meristems, including IM, TSM, SM, and floret meristem (FM) throughout the spikelet differentiation phase, were devoid of *HvALOG1* signals (Figures 4B–4K). As expected, *HvALOG1* mRNA was absent from all stages or tissues in *flo.a* samples, consistent with the gene deletion (Figure S4A).

For protein analyses, we first investigated the subcellular localization of HvALOG1 and found the HvALOG1-GFP signals restricted to the nucleus of barley leaf cells, while the control GFP protein was distributed throughout the cells (Figure S4B). This identifies HvALOG1 as a nucleus-targeted protein that may function as a transcriptional regulator. Subsequently, we generated a GFP reporter line (*HvALOG1-p*:HvALOG1:GFP) to investigate the expression pattern of HvALOG1 protein during various spike development stages. Consistent with our mRNA *in situ* hybridization results, GFP signals were absent from reproductive meristems. However, a broad protein localization was observed in other areas, such as LR primordia and rachis tissue (Figures S4C–S4L), which may be attributable to various factors, including protein transport. As spikelet initiation progressed, GFP signals were observed at the base of emerging floret organs, potentially marking organ boundaries (Figures S4L6–S4L9). At the AP stage, GFP signals were limited to the rachis and boundary domain of floret organs (Figures S4M–S4S).

These results suggest that during spike development, HvALOG1 is expressed in non-meristematic reproductive tissues and subsequently at the base of floret primordia following spikelet initiation. Therefore, HvALOG1 may have an essential role in specifying the determinacy of the barley SM in a non-cell-autonomous manner by modulating proper boundary establishment. Proper floret organ development, however, is accomplished in a cell-autonomous manner.

Role of HvALOG1 in organ boundary formation and developmental regulation

To further unravel the molecular signatures associated with the observed extra spikelet initiation and CS glume fusion in the upper-mid inflorescence in the absence of *HvALOG1*, we conducted RNA-seq analysis to investigate the transcriptomic differences in developing inflorescence tissues (whole spike at the DR [Waddington scale 2.0, W2.0)[43] and split spike (upper-mid and basal parts at LP [W3.0], AP [W4.5], and WA [5.5] stages) from BW and *flo.a* (Figure S5A). Consistent with the emergence of extra organs in *flo.a* at the LP stage, principal component analysis using all 42 samples revealed significant transcriptome modulation starting from the LP stage (Figure 5A). The distribution of samples followed the trajectory of inflorescence development (DR to WA) and positional distribution (upper-mid to basal) (Figure 5A). Transcriptomes of all BW and *flo.a* samples were clustered together at the DR and WA stages but were separated at the LP and AP stages, indicating remarkable gene expression alterations between the upper-mid and basal parts of the spike in BW and *flo.a* (Figure 5A).

A total of 3,158 differentially expressed genes (DEGs) were detected in *flo.a* versus BW (Figure S5B; Table S1). Most of these DEGs were identified at the LP stage (62.92%), indicating strong ectopic transcriptomic activity contributing to the formation of extra spikelets in *flo.a* (Figure S5B). Upregulated DEGs outnumbered downregulated ones, suggesting that HvALOG1 could function as a transcriptional repressor (Figure S5B). *HvALOG1* transcripts were abundant in the whole spike of BW samples but completely absent in the *flo.a* spike (Figure S5C). The absence of extra spikelets in the basal part of *flo.a* spikes suggests that a specific pathway or gene redundancy rescued the *flo.a* phenotype during the formation of basal spikelets, which differentiate during the DR stage. Additionally, 1,326 and 973 genes were differentially expressed between LP-basal and AP-basal, respectively, indicating that *HvALOG1* may also participate in other pathways that regulate spike development (Figure S5B). Expression clustering analysis revealed that the DEGs can be divided into eight groups (C1 to C8) (Figure S5D). Given the observation that extra SMs emerge during the LP stage, particular attention was directed toward genes within clusters C4 and C6, which showed specific differential expression patterns in the upper middle and base parts of the spikes at the LP stage (Figure 5B). Gene ontology (GO) enrichment analysis showed that DEGs in group C4 were enriched with functions related to shoot system development, plant organ formation, floral whorl development, and auxin homeostasis, while DEGs in group C6 were primarily associated with stress response and biosynthesis of metabolites (Figure 5C; Table S2).

The most pronounced expression differences were observed at the LP and AP stages, where the expression of a set of genes involved in organ boundary formation, including *CUC2*,[44] *KNOTTED-LIKE FROM ARABIDOPSIS THALIANA/BREVIPEDICELLUS* (*KNAT1/BP*)*-like 1*,[45] *KNAT1/BP-like 2*, *LIGULELESS 1* (*HvLG1*),[46] *SUPERMAN* (*SUP*)*-like*,[47] *ARABIDOPSIS THALIANA HOMEOBOX 1* (*ATHB1*),[48] *PERIANTHIA* (*PAN*),[49] and *LATERAL*

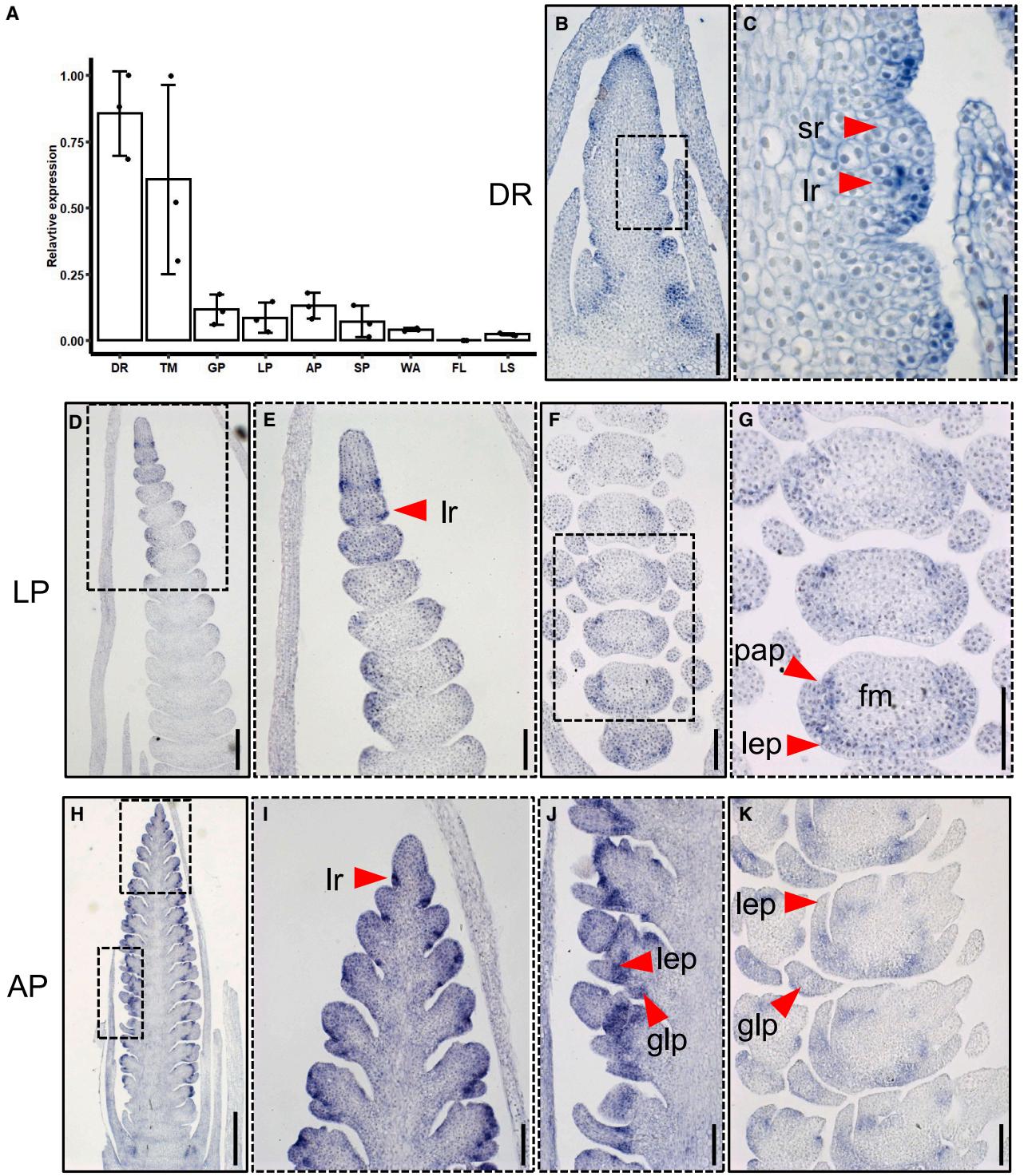

Figure 4. Temporal and spatial expression pattern of *HvALOG1*

(A) Relative expression by qRT-PCR of *HvALOG1* in different vegetative and reproductive tissues. *HvActin* was used for expression normalization. Data are shown as mean ± SD; biological replicates = 3; DR, double ridge; TM, triple mound; GP, glume primordium; LP, lemma primordium; SP, stamen primordium; AP, awn primordium; WA, white anther; FL, flag leaf in awn primordium stage; LS, leaf sheath in awn primordium stage.

(B–K) Representative images of mRNA *HvALOG1* expression domains in BW developing inflorescence by mRNA *in situ* hybridization. The enlarged image of the dotted box is shown on the right. fm, floral meristem; glp, glume primordium; lep, lemma primordium; lr, leaf ridge; pap, palea primordium; sr, spike ridge. Scale bar, 50 μm (C); 100 μm (B, E–G, and I–K); 200 μm (D); 500 μm (H).

See also Figure S4.

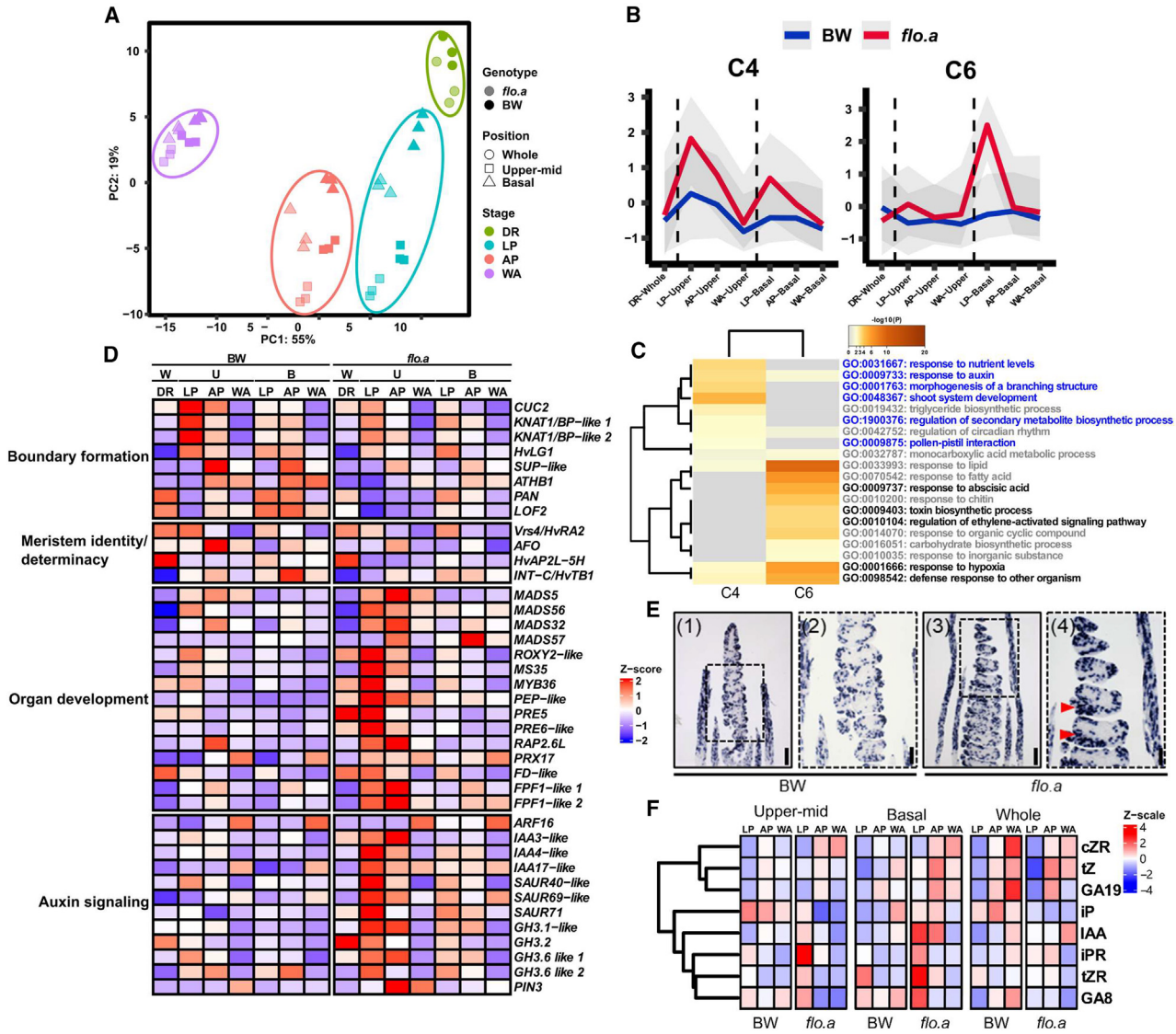

Figure 5. *HvALOG1*-related transcriptional changes affect the boundary formation of floral organ

(A) Principal component analysis (PCA) on the expression-filtered transcriptomes illustrates the variation between BW and *flo.a* from different spike sections at the DR, LP, AP, and WA stages.

(B) Clustering analysis (C4 and C6) of DEGs based on partition around medoids (PAM) using normalized expression value (*Z* score). The blue and red lines indicate median expression; the gray area represents the 5th and 95th quantile.

(C) Gene Ontology (GO) analysis of clusters 4 (C4) and 6 (C6) shows specific expression in the upper-mid and basal parts of spikes at the LP stage.

(D) Heatmap of the selected candidate genes with roles in organ boundary formation, meristem identity/determinacy, auxin homeostasis, and organ development using *Z* score value.

(E) Representative images of *Histone4* (*H4*) expression pattern in developing inflorescence of BW and *flo.a* by mRNA *in situ* hybridization at the SP stage. (2) and (4) are enlarged images of (1) and (3), respectively. Red arrowheads indicate extra meristem/primordium events. Scale bar, 100 μm (2 and 4); 200 μm (1 and 3).

(F) Phytohormone profiling from developing inflorescence. Auxi, indole-3-acetic acid (IAA); gibberellins, GA8 and GA19; cytokinins, N6-isopentenyladenine (iP), N(6)-isopentenyladenosine (iPR), trans-Zeatin-O-glucoside (tZR), cis-Zeatin-riboside (cZR), and trans-Zeatin (tZ).

W, whole spike; U, upper-mid; B, basal.

See also Figure S5 and Tables S1, S2, S3, and S4.

ORGAN FUSION2 (*LOF2*),[50] was downregulated in *flo.a*, in line with the inability of *flo.a* spikelets to correctly establish boundaries in meristems or primordia (Figure 5D; Table S3). Moreover, expression of genes involved in the specification of spikelet identity or determinacy, including *RAMOSA2* (*HvRA2*)/*Vrs4*,[51] *Arabidopsis ABNORMAL FLORAL ORGANS/FILAMENTOUS FLOWER* (*AFO/FIL*),[52,53] *APETALA2-like transcription factor* (*HvAP2L-H5*),[54] and *Intermedium-spike c* (*Int-C*)/*HvTB1*,[55] was similarly downregulated in the upper-mid part of the *flo.a* spike (Figure 5D; Table S3). In contrast, the expression of genes involved in the auxin signaling pathway, such as *Auxin response factor 16* (*ARF16*), *AUXIN/INDOLE-3-ACETIC ACID* (*AUX/IAA*), *Small Auxin*

Up-Regulated RNA (*SAUR*), *GRETCHEN HAGEN3* (*GH3*), and *PIN-FORMED 3* (*PIN3*), was specifically upregulated in the upper-mid spike of *flo.a*[56–60] (Figure 5D; Table S3). Another group of genes related to organ development, such as *MADS-box* (*5*, *56*, *32*, and *57*),[61] *PACLOBUTRAZOL-RESISTANCE 5* and *6* (*PRE5* and 6),[62] and *FD*,[63] were also specifically highly expressed in the upper-mid part of spike of *flo.a*, possibly due to the absence of repression from downregulated genes mentioned above (Figure 5D; Table S3).

We hypothesized that the emergence of extra spikelets in *flo.a* may be related to ectopic cell division. RNA-seq data showed a modest upregulation of *HISTONE H4* (*H4*), a marker for active cell division, in the upper-mid part of the *flo.a* spike (Figure S5E). This was further substantiated by mRNA *in situ* hybridization analysis of *H4*, which revealed a strong signal in the domain below the CS from the upper-mid part of the *flo.a* spike, indicating newly forming meristems (Figures 5E and S5F). Furthermore, the expression of multiple genes involved in cell division was altered in *flo.a* young spikes, including *cell division cycle*, *cyclin*, and *histone* genes, as shown by RNA-seq analysis (Figure S5G). Meanwhile, the phytohormonal measurements revealed that significant phytohormonal shifts occurred between BW and *flo.a* spikes (Figure 5F; Table S5). Correspondingly, a group of genes related to hormone signaling pathways was differentially expressed in young spike tissues between BW and *flo.a* (Figure S5H).

Therefore, we conclude that HvALOG1 is essential for the specification of proper spikelet growth during inflorescence development by coordinating gene expression related to cell division activity, spikelet identity/determinacy, boundary formation, organ growth, and hormone signaling, thereby preventing the development of ectopic spikelet-associated organs.

Barley ALOG family members display functional redundancy during early spike development

ALOG family members have been shown to act synergistically in tomato to precisely control SAM maturation, synchronized flowering, and compound inflorescence production.[30] Given this context, we hypothesized that *ALOG* genes in barley exert conserved molecular functions but with spatiotemporal specificity to regulate SM determinacy and organ boundary formation. *HvALOG1* and its closest paralog *HvALOG2* on chromosome 7H belong to phylogenetic clade 2 (Figure S3G) and display similar expression trends in whole immature spike tissues (Figure S6A).[64] We explored the potential for functional redundancy or a dosage effect stemming from these two paralogs. Single and double mutants were generated by incorporating two single-guide RNAs targeting the exonic regions of *HvALOG1* and *HvALOG2*, respectively, into the same binary vector for Cas9-mediated genome editing (Figure S6B). In the second-generation (T_1) transgenic plants, we identified homozygous indel mutations in *HvALOG1* and *HvALOG2*, although *HvALOG1* target 1 displayed low editing efficiency (Figure S6B). In *Hvalog2* single knockout transgenic plants (*ALOG1*/*alog2*^{CR}), spike and spikelet phenotypes were not significantly altered compared to null transgenic control lines (Figure S6C), indicating that *HvALOG2* has a negligible impact on suppressing the formation of ectopic organs. However, the double mutant of *Hvalog1* and *Hvalog2* (*alog1*^{CR}/*alog2*^{CR}) displayed more pronounced *flo* phenotypes in the upper-mid parts of the spike, not only producing an extra spikelet but also causing CS glumes to transform into organs with varying degrees of development, ranging from a leaf-like state to complete florets featuring lemma, palea, stamens, and ovary (Figures 6A, 6B, 6E, and 6F). Surprisingly, in the double knockouts, the differentiation of the TSM was halted in the upper-mid part of the inflorescence, losing the ability to produce spikelets, and the development of the upper glume of LSs was inhibited (Figures 6C, 6D, and 6F). Notably, among 190 transgenic plants, no single *Hvalog1* mutant (*alog1*^{CR}/*ALOG2*) was detected, primarily due to the high gene editing efficiency of target 1 and 2 for *HvALOG2*. The *alog1*^{CR}/*alog2*^{CR} double mutant displayed enhanced *flo* phenotypes, implying that these two ALOG proteins work redundantly or in a similar pathway to regulate inflorescence morphogenesis.

In our RNA-seq data, *HvALOG1* exhibited the highest expression in whole BW spike tissue at the DR stage and was the only gene expressed in all developing stages, suggesting its key role in regulating SM activity and boundary establishment (Figure 6G). In contrast, genes in clades 1 to 3 (Figure S3G), excluding *HvALOG1*, displayed spatiotemporal and tissue-specific expression patterns with high expression in whole spikes at the DR stage but very low expression in the upper-mid part at the LP stage (Figure 6G). Additionally, mRNA *in situ* hybridization assays showed that *HvALOG4*, a representative of clade 3, had high mRNA accumulation in whole spike tissues at the DR stage (Figure 6H). These findings suggest that the positional distribution of *flo* mutant phenotypes along the spike may be derived from imbalances in spatiotemporal expression dynamics of ALOG family members. Different ALOG members, including *HvALOG1*, may synergistically regulate SM activity and confer SM determinacy during the early developmental stage (DR). However, the absence of *HvALOG1* expression leads to an indeterminate SM, but only in the upper-mid portion of the spike during later stages (LP and AP) when *HvALOG1* is the only expressed gene of the ALOG family (Figures 6G and 7).

Thus, we propose that the barley ALOG protein family might work synergistically to regulate inflorescence shape. Among all ALOG family members *HvALOG1* plays a dominant role in specifying SM determinacy and maintaining boundary formation. The loss of *HvALOG1* might be compensated for by other ALOG proteins in more basal spike parts, resulting in the positional patterning of the *flo.a* mutant spike.

Effect of extra spikelet inflorescence architecture on yield-related traits

To further explore the impact of the modified inflorescence shape on yield-related traits and potential breeding value under varying environmental conditions, we assessed spike grain yields from plants cultivated in both greenhouse and field environments (Figures 1A, 1B, and S7A). The inflorescences generated by *flo.a* plants in both settings exhibited multiple extra spikelet units. The *flo.a* plants performed better in the field compared to the greenhouse, producing more extra spikelets, normal CSs, and grains (Figures S7B–S7D). However, in comparison to BW, *flo.a* produced fewer CSs and grains per inflorescence under both conditions (Figures S7B–S7D).

Greenhouse-grown *flo.a* plants displayed a significant decrease in yield-related traits, including grain size and

CellPress
OPEN ACCESS

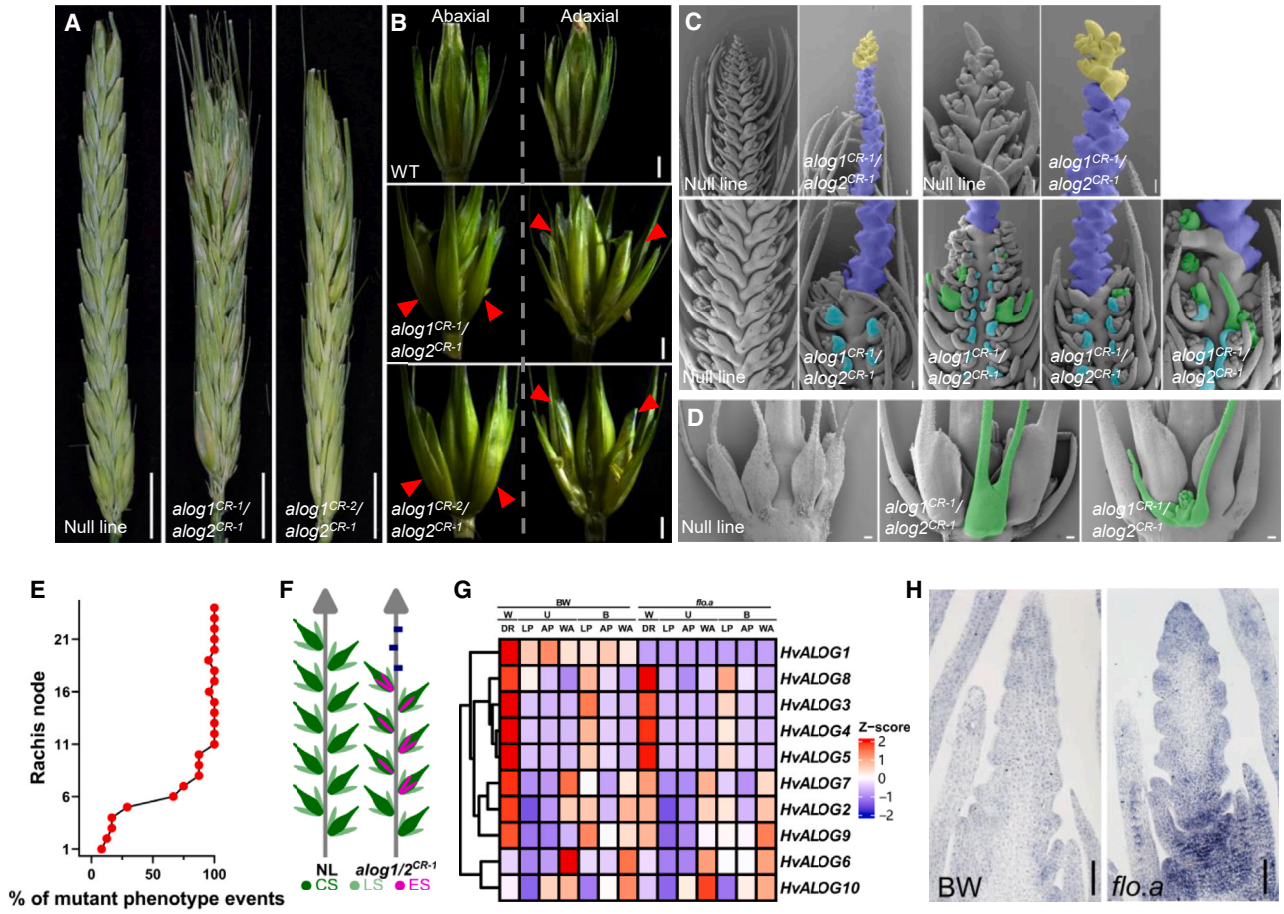

Figure 6. Proposed redundant functions of ALOG proteins may rescue *flo* phenotypes in basal spike regions

(A and B) Representative inflorescence (A) and triple spikelet (B) images from Golden Promise and engineered *Hvalog1* and *Hvalog2* double mutant. Red arrowheads indicate floret converted from CS glume. Scale bar, 1 cm (A); 1 mm (B).

(C and D) SEM images of the developing spike (C) and triple spikelets (D) from null line and the double mutants. Yellow areas indicate apical domain of spike of double mutant. Dark blue areas indicate the spike rachis with arrested TSM. Light blue areas indicate the suppressed LS glume. Green areas indicate the *flo.a* phenotype event. Scale bar, 100 μm.

(E) Phenotypic distribution of extra spikelet and fused glume in the *Hvalog1* and *Hvalog2* double mutant.

(F) Schematic diagram of the phenotype differences between null line and the *Hvalog1* and *Hvalog2* double mutant.

(G) Expression pattern of ten members of barley ALOG family based on RNA-seq data.

(H) Representative images of *HvALOG4* expression pattern in developing inflorescence of BW and *flo.a* by mRNA *in situ* hybridization at the DR stage. Scale bar, 100 μm.

See also Figure S6.

thousand-grain weight. In contrast, under field conditions, *flo.a* and BW demonstrated nearly equivalent performance (Figures S7E and S7F). Overall, these findings suggest that the loss of *HvALOG1* led to extra spikelet formation but did not significantly affect grain yield of the individual spike. Genetic manipulation of the floral organ fate pathway to confer fertility toward extra spikelets may possibly contribute to yield enhancement without affecting primary spikelet development.[65]

DISCUSSION

The inflorescence architecture of crop plants is predominantly regulated by two factors, meristem activity and fate, both of which play a critical role in determining the number of spikelets per inflorescence for grain production. Genetic manipulation aimed at modifying meristems represents a promising approach for flexible inflorescence modifications, offering the potential for enhancing crop yields.[2,66–68] Here, we characterized a barley extra spikelet mutant, *flo.a*, which produced extra sterile spikelets and fused glumes abaxially to the CS. We found that HvALOG1 displays a boundary-specific expression pattern, thereby providing developmental signals to specify the growth of spikelet and floret organs. Moreover, our data suggest that HvALOG1 and HvALOG2 cooperatively regulate inflorescence morphogenesis, and the unequal redundant roles of this ALOG family may be related to the positional distribution of the mutant phenotype. These findings reveal a critical role for ALOG proteins in directing inflorescence architecture through the regulation of SM fate and activity in barley.

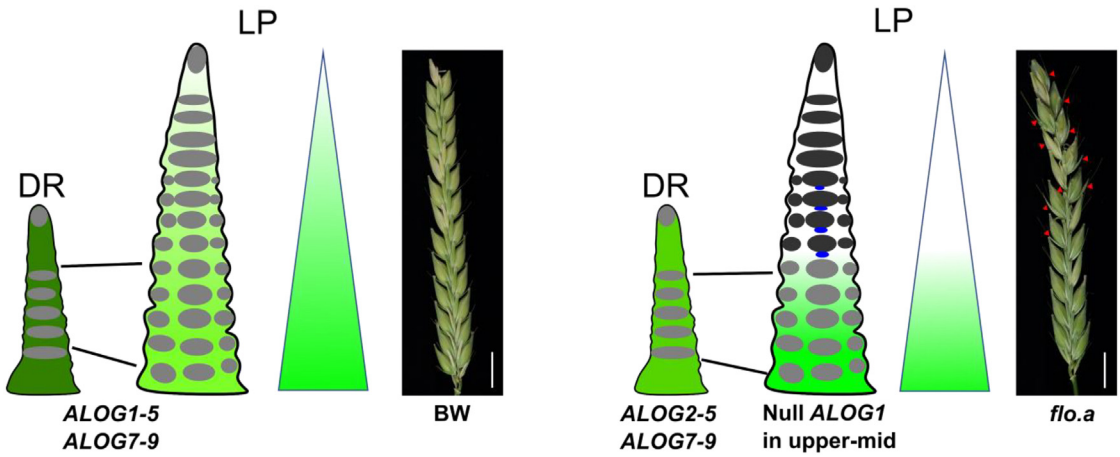

Figure 7. The proposed regulatory mechanism of ALOG family members for mediating SM determinacy

Different degrees of green indicate expression levels of ALOG members in spike tissues. The red triangles indicate the *flo.a* events. Light and dark gray ovals represent unaffected and affected reproductive meristems, respectively. Blue ovals represent additional spikelet meristems. DR, double ridge; LP, lemma primordium. Scale bar, 1 cm.

ALOG genes are broadly involved in boundary establishment, organogenesis, and inflorescence development.[19,20,22–34] Phenotypically, mutations in *HvALOG1* result in the production of extra spikelets sharing the same rachis node with the regular spikelet triplet to form spikelet quadruplets, suggesting deprivation of SM determinacy of CSs (Figures 1, 2, and S1). In *Arabidopsis*, *LSH3* and *LSH4* exhibit boundary-specific expression and regulate lateral organ differentiation.[19,69] In rice and sorghum, ALOG members are involved in regulating the transition from indeterminate to determinate meristem, and spikelet/floret specification and development.[22,23,25,27,29,32,34] In a parallel study on the ALOG family in wheat,[70] the authors revealed that the wheat (i.e., *ALOG-1*) ortholog of *HvALOG1* is involved in the regulation of inflorescence development; consistent with this, absence of *ALOG-1* in wheat facilitates formation of a secondary spikelet immediately below the primary spikelet, indicating a conserved role for ALOG in restricting the boundary of spikelet formation in Triticeae. Formally, *HvALOG1* may contribute to the canonical developmental program of spikelet triplets by repressing ectopic organ formation in barley. Notably, expression of HvALOG1 is specifically absent from any reproductive meristem, demonstrating a non-cell-autonomous regulatory mechanism of SM activity (Figures 4 and S4C–S4S). Consistent with our observation, in wheat, *ALOG-1* influenced by *PHOTOPERIOD-1* is expressed in the developing inflorescence and is specifically restricted to the leaf ridge.[70] This boundary-centered expression and subsequent signaling is essential for determining meristem fate and appears as a widespread regulatory mechanism in grasses.[11] Conversely, CS glumes of *flo.a* fuse into leaf-like structures, suggesting disrupted floral organ boundaries and partially lost CS glume identity (Figures 1B and 1C), consistent with boundary formation defects in other plants. We thus hypothesize that HvALOG1, expressed at the base of floret organ primordia, regulates floret organ development in a cell-autonomous manner.

Positional distribution of *flo.a* phenotypes may be related to incomplete redundancies with ALOG family members. Recent studies in tomato have shown that *TERMINAL FLOWER* and its paralogs work together to regulate the production of compound inflorescences.[30,31] Considering that *HvALOG1* is entirely deleted in *flo.a*, its function in maintaining meristem activity may be exerted by other spatially and temporally co-expressed ALOG paralogs that rescue mutant phenotypes in the basal part of spike. The deletion of *HvALOG1* and the weak expression of other paralogs may create incongruent determinacy signals during the formation and differentiation of SMs in the upper-mid parts of the *flo.a* spike, resulting in extra spikelets and organ fusion phenotypes (Figures 6E–6G and 7). We hypothesize that other barley ALOG proteins might provide an unidentified level of genetic redundancy to maintain spike meristem activity, particularly during early spike development (Figure 7). In wheat, secondary spikelets of the *alog-1* are mainly formed in the central region of the inflorescence, suggesting that the specification for spikelet development appears to be regulated by spatiotemporal development.[70]

At the cellular level, HvALOG1 functions by regulating cell-cycle/division activity. In *flo.a*, the extra spikelets generated from the boundary between the CS and the rachis may be related to ectopic cell division activity (Figures 5E, S5E, and S5F). The production of extra spikelets is controlled by multiple genes; e.g., wheat *PHOTOPERIOD-1*, *FLOWERING LOCUS T1*, *TEOSINTE BRANCHED1*, *HOMEOBOX DOMAIN-2*, and *DUO-B1* control the initiation of additional spikelets by regulating the activity of the axillary meristem.[4,7,8,10] Our transcriptomic data showed that the expression of boundary establishment-related genes is downregulated in *flo.a*, thereby promoting cell division activity and causing delayed or leaky boundary establishment between CS glumes (Figure 5D). Moreover, meristem identity/determinacy-associated genes, including *Vrs4/HvRA2*,[51] *AFO*,[52,53] *HvAP2L-5H*,[54] and *INT-C/HvTB1*,[55] were downregulated in *flo.a*, with misexpression disrupting meristem stability and altering cell proliferation or differentiation (Figure 5D). In contrast, genes related to cell division, bud development, and floral organogenesis were upregulated in upper-mid *flo.a* spike tissue, possibly linked to ectopic floral organogenesis (Figure 5D). At

the hormone level, we observed differential expression of genes involved in hormone signaling pathways (Figures 5D and S5H); consistently, accumulation of key plant hormones was significantly altered in BW and *flo.a*, resulting in disruption of hormone homeostasis (Figure 5F). Specifically, auxin accumulation was higher in the upper-mid *flo.a* spikes (Figure 5F), consistent with the extra spikelet and glume fusion phenotype (Figures 1A–1C).

In conclusion, we show that mutations in *HvALOG1* lead to the production of extra spikelets and are linked to the fusion of floral organs derived from boundary loss. HvALOG1 plays a crucial role in maintaining the inflorescence architecture in barley, both by non-cell-autonomously determining the SM determinacy and by autonomously controlling the formation of boundaries between spikelet organs. Our study offers new insights into the function of ALOG family members in regulating meristem activity and inflorescence development in barley. The positional effect of mutant phenotypes along the spike emphasizes unequal spatio-temporal redundancies among ALOG members in regulating spikelet development. These findings may contribute to our understanding of the molecular mechanisms underlying inflorescence development and may have implications for crop improvement.

STAR★METHODS

Detailed methods are provided in the online version of this paper and include the following:

- KEY RESOURCES TABLE
- RESOURCE AVAILABILITY
  - Lead contact
  - Materials availability
  - Data and code availability
- EXPERIMENTAL MODEL AND SUBJECT DETAILS
- METHOD DETAILS
  - Barley phenotyping
  - WGS and introgression identification
  - Genetic analysis and map-based cloning
  - Inducing targeted knock-out mutations
  - Construction of GFP reporter plants
  - Scanning electron microscopy analysis
  - mRNA isolation and qRT-PCR
  - RNA sequencing
  - RNA-seq data analysis
  - Phylogenetic analysis
  - Phytohormone measurements
  - Subcellular localization
  - Light microscopy
  - 3D reconstruction
  - mRNA *in situ* hybridization
- QUANTIFICATION AND STATISTICAL ANALYSIS

SUPPLEMENTAL INFORMATION

Supplemental information can be found online at https://doi.org/10.1016/j.cub.2024.04.083.

ACKNOWLEDGMENTS

The authors would like to thank C. Trautewig, K. Wolf, S. Sommerfeld, E. Weiss, and M. Pürschel for excellent technical assistance; S. Zhao for contributions to the mRNA *in situ* hybridization assay; R. Hoffie for assisting in barley transformation; A. Fiebig and M. Maruschewski for bioinformatics support and data submission; D. Boehmert and B. Kettig for phytohormone measurement; and all members from the Plant Architecture Lab for fruitful discussions. G.J. is holder of a Chinese Scholarship Council (CSC) fellowship (no. 201706910077). While conducting this study, T.S. received financial support from the HEISENBERG Program of the German Research Foundation (DFG), grant no SCHN 768/15-1. The authors would also like to thank IPK for providing core budget funding and an excellent research infrastructure.

AUTHOR CONTRIBUTIONS

T.S. conceived the idea and supervised the study. G.J. and T.S. designed the experiments. R.K. and Y.H. expanded the idea and guided the study direction. G.J. carried out most of the phenotyping, mapping, sampling, molecular experiments, and data analysis. Y.A.T.M. and N.v.W. led hormone profiling. T.R. conducted most of the microscopy observations. G.H. and J.K. led and guided the barley transformation. J.R. performed the subcellular localization experiment. M.M. conducted whole-genome sequencing data analysis. G.J. wrote the original draft of the manuscript and T.S. revised and edited previous versions of the manuscript. All authors approved the final version of the paper.

DECLARATION OF INTERESTS

The authors declare no competing interests.

Received: November 16, 2023
Revised: March 18, 2024
Accepted: April 30, 2024
Published: May 22, 2024

REFERENCES

1. Zhu, Y., and Wagner, D. (2020). Plant inflorescence architecture: the formation, activity, and fate of axillary meristems. Cold Spring Harb. Perspect. Biol. *12*, a034652. https://doi.org/10.1101/cshperspect.a034652.
2. Koppolu, R., and Schnurbusch, T. (2019). Developmental pathways for shaping spike inflorescence architecture in barley and wheat. J. Integr. Plant Biol. *61*, 278–295. https://doi.org/10.1111/jipb.12771.
3. Zhang, D., and Yuan, Z. (2014). Molecular control of grass inflorescence development. Annu. Rev. Plant Biol. *65*, 553–578. https://doi.org/10.1146/annurev-arplant-050213-040104.
4. Boden, S.A., Cavanagh, C., Cullis, B.R., Ramm, K., Greenwood, J., Jean Finnegan, E., Trevaskis, B., and Swain, S.M. (2015). Ppd-1 is a key regulator of inflorescence architecture and paired spikelet development in wheat. Nat. Plants *1*, 14016. https://doi.org/10.1038/nplants.2014.16.
5. Li, G., Kuijer, H.N.J., Yang, X., Liu, H., Shen, C., Shi, J., Betts, N., Tucker, M.R., Liang, W., Waugh, R., et al. (2021). MADS1 maintains barley spike morphology at high ambient temperatures. Nat. Plants *7*, 1093–1107. https://doi.org/10.1038/s41477-021-00957-3.
6. Poursarebani, N., Seidensticker, T., Koppolu, R., Trautewig, C., Gawroński, P., Bini, F., Govind, G., Rutten, T., Sakuma, S., Tagiri, A., et al. (2015). The genetic basis of composite spike form in barley and 'miracle-wheat'. Genetics *201*, 155–165. https://doi.org/10.1534/genetics.115.176628.
7. Dixon, L.E., Pasquariello, M., Badgami, R., Levin, K.A., Poschet, G., Ng, P.Q., Orford, S., Chayut, N., Adamski, N.M., Brinton, J., et al. (2022). MicroRNA-resistant alleles of *HOMEOBOX DOMAIN-2* modify inflorescence branching and increase grain protein content of wheat. Sci. Adv. *8*, eabn5907. https://doi.org/10.1126/sciadv.abn5907.
8. Dixon, L.E., Greenwood, J.R., Bencivenga, S., Zhang, P., Cockram, J., Mellers, G., Ramm, K., Cavanagh, C., Swain, S.M., and Boden, S.A. (2018). TEOSINTE BRANCHED1 regulates inflorescence architecture and development in bread wheat (Triticum aestivum). Plant Cell *30*, 563–581. https://doi.org/10.1105/tpc.17.00961.
9. Koppolu, R., Jiang, G., Milner, S.G., Muqaddasi, Q.H., Rutten, T., Himmelbach, A., Guo, Y., Stein, N., Mascher, M., and Schnurbusch, T. (2022). The barley mutant multiflorus2.b reveals quantitative genetic

variation for new spikelet architecture. Theor. Appl. Genet. *135*, 571–590. https://doi.org/10.1007/s00122-021-03986-w.

10. Wang, Y., Du, F., Wang, J., Wang, K., Tian, C., Qi, X., Lu, F., Liu, X., Ye, X., and Jiao, Y. (2022). Improving bread wheat yield through modulating an unselected AP2/ERF gene. Nat. Plants *8*, 930–939. https://doi.org/10.1038/s41477-022-01197-9.
11. Whipple, C.J. (2017). Grass inflorescence architecture and evolution: the origin of novel signaling centers. New Phytol. *216*, 367–372. https://doi.org/10.1111/nph.14538.
12. Yu, H., and Huang, T. (2016). Molecular mechanisms of floral boundary formation in Arabidopsis. Int. J. Mol. Sci. *17*, 317. https://doi.org/10.3390/ijms17030317.
13. Žádníková, P., and Simon, R. (2014). How boundaries control plant development. Curr. Opin. Plant Biol. *17*, 116–125. https://doi.org/10.1016/j.pbi.2013.11.013.
14. Aida, M., and Tasaka, M. (2006). Genetic control of shoot organ boundaries. Curr. Opin. Plant Biol. *9*, 72–77. https://doi.org/10.1016/j.pbi.2005.11.011.
15. Wang, Q., Hasson, A., Rossmann, S., and Theres, K. (2016). Divide et impera: boundaries shape the plant body and initiate new meristems. New Phytol. *209*, 485–498. https://doi.org/10.1111/nph.13641.
16. Aida, M., Ishida, T., Fukaki, H., Fujisawa, H., and Tasaka, M. (1997). Genes involved in organ separation in Arabidopsis: an analysis of the cup-shaped cotyledon mutant. Plant Cell *9*, 841–857. https://doi.org/10.1105/tpc.9.6.841.
17. Takada, S., Hibara, K., Ishida, T., and Tasaka, M. (2001). The CUP-SHAPED COTYLEDON1 gene of Arabidopsis regulates shoot apical meristem formation. Development *128*, 1127–1135.
18. Vroemen, C.W., Mordhorst, A.P., Albrecht, C., Kwaaitaal, M.A.C.J., and De Vries, S.C. (2003). The CUP-SHAPED COTYLEDON3 gene is required for boundary and shoot meristem formation in Arabidopsis. Plant Cell *15*, 1563–1577. https://doi.org/10.1105/tpc.012203.
19. Cho, E., and Zambryski, P.C. (2011). ORGAN BOUNDARY1 defines a gene expressed at the junction between the shoot apical meristem and lateral organs. Proc. Natl. Acad. Sci. USA *108*, 2154–2159. https://doi.org/10.1073/pnas.1018542108.
20. Takeda, S., Hanano, K., Kariya, A., Shimizu, S., Zhao, L., Matsui, M., Tasaka, M., and Aida, M. (2011). CUP-SHAPED COTYLEDON1 transcription factor activates the expression of LSH4 and LSH3, two members of the ALOG gene family, in shoot organ boundary cells. Plant J. *66*, 1066–1077. https://doi.org/10.1111/j.1365-313X.2011.04571.x.
21. Hepworth, S.R., and Pautot, V.A. (2015). Beyond the divide: boundaries for patterning and stem cell regulation in plants. Front. Plant Sci. *6*, 1052. https://doi.org/10.3389/fpls.2015.01052.
22. Beretta, V.M., Franchini, E., Ud Din, I., Lacchini, E., Van den Broeck, L., Sozzani, R., Orozco-Arroyo, G., Caporali, E., Adam, H., Jouannic, S., et al. (2023). The ALOG family members OsG1L1 and OsG1L2 regulate inflorescence branching in rice. Plant J. *115*, 351–368. https://doi.org/10.1111/tpj.16229.
23. Yoshida, A., Suzaki, T., Tanaka, W., and Hirano, H.-Y. (2009). The homeotic gene long sterile lemma (G1) specifies sterile lemma identity in the rice spikelet. Proc. Natl. Acad. Sci. USA *106*, 20103–20108. https://doi.org/10.1073/pnas.0907896106.
24. Bencivenga, S., Serrano-Mislata, A., Bush, M., Fox, S., and Sablowski, R. (2016). Control of oriented tissue growth through repression of organ boundary genes promotes stem morphogenesis. Dev. Cell *39*, 198–208. https://doi.org/10.1016/j.devcel.2016.08.013.
25. Li, X., Sun, L., Tan, L., Liu, F., Zhu, Z., Fu, Y., Sun, X., Sun, X., Xie, D., and Sun, C. (2012). TH1, a DUF640 domain-like gene controls lemma and palea development in rice. Plant Mol. Biol. *78*, 351–359. https://doi.org/10.1007/s11103-011-9868-8.
26. Macalister, C.A., Park, S.J., Jiang, K., Marcel, F., Bendahmane, A., Izkovich, Y., Eshed, Y., and Lippman, Z.B. (2012). Synchronization of the flowering transition by the tomato TERMINATING FLOWER gene. Nat. Genet. *44*, 1393–1398. https://doi.org/10.1038/ng.2465.
27. Peng, P., Liu, L., Fang, J., Zhao, J., Yuan, S., and Li, X. (2017). The rice TRIANGULAR HULL1 protein acts as a transcriptional repressor in regulating lateral development of spikelet. Sci. Rep. *7*, 13712. https://doi.org/10.1038/s41598-017-14146-w.
28. Xu, C., Park, S.J., Van Eck, J., and Lippman, Z.B. (2016). Control of inflorescence architecture in tomato by BTB/POZ transcriptional regulators. Genes Dev. *30*, 2048–2061. https://doi.org/10.1101/gad.288415.116.
29. Yoshida, A., Sasao, M., Yasuno, N., Takagi, K., Daimon, Y., Chen, R., Yamazaki, R., Tokunaga, H., Kitaguchi, Y., Sato, Y., et al. (2013). TAWAWA1, a regulator of rice inflorescence architecture, functions through the suppression of meristem phase transition. Proc. Natl. Acad. Sci. USA *110*, 767–772. https://doi.org/10.1073/pnas.1216151110.
30. Huang, X., Xiao, N., Zou, Y., Xie, Y., Tang, L., Zhang, Y., Yu, Y., Li, Y., and Xu, C. (2022). Heterotypic transcriptional condensates formed by prion-like paralogous proteins canalize flowering transition in tomato. Genome Biol. *23*, 78. https://doi.org/10.1186/s13059-022-02646-6.
31. Huang, X., Chen, S., Li, W., Tang, L., Zhang, Y., Yang, N., Zou, Y., Zhai, X., Xiao, N., Liu, W., et al. (2021). ROS regulated reversible protein phase separation synchronizes plant flowering. Nat. Chem. Biol. *17*, 549–557. https://doi.org/10.1038/s41589-021-00739-0.
32. Zhou, L., Zhu, C., Fang, X., Liu, H., Zhong, S., Li, Y., Liu, J., Song, Y., Jian, X., and Lin, Z. (2021). Gene duplication drove the loss of awn in sorghum. Mol. Plant *14*, 1831–1845. https://doi.org/10.1016/j.molp.2021.07.005.
33. Zhao, L., Nakazawa, M., Takase, T., Manabe, K., Kobayashi, M., Seki, M., Shinozaki, K., and Matsui, M. (2004). Overexpression of LSH1, a member of an uncharacterised gene family, causes enhanced light regulation of seedling development. Plant J. *37*, 694–706. https://doi.org/10.1111/j.1365-313x.2003.01993.x.
34. Sato, D.-S., Ohmori, Y., Nagashima, H., Toriba, T., and Hirano, H.-Y. (2014). A role for TRIANGULAR HULL1 in fine-tuning spikelet morphogenesis in rice. Genes Genet. Syst. *89*, 61–69.
35. Beretta, V.M., Franchini, E., Ud Din, I., Lacchini, E., Van den Broeck, L., Sozzani, R., Orozco-Arroyo, G., Caporali, E., Adam, H., Jouannic, S., et al. (2023). The ALOG family members OsG1L1 and OsG1L2 regulate inflorescence branching in rice. Plant J. *115*, 351–368. https://doi.org/10.1111/tpj.16229.
36. Thirulogachandar, V., and Schnurbusch, T. (2021). 'Spikelet stop' determines the maximum yield potential stage in barley. J. Exp. Bot. *72*, 7743–7753. https://doi.org/10.1093/jxb/erab342.
37. Druka, A., Franckowiak, J., Lundqvist, U., Bonar, N., Alexander, J., Houston, K., Radovic, S., Shahinnia, F., Vendramin, V., Morgante, M., et al. (2011). Genetic dissection of barley morphology and development. Plant Physiol. *155*, 617–627. https://doi.org/10.1104/pp.110.166249.
38. Huang, Y., Kamal, R., Shanmugaraj, N., Rutten, T., Thirulogachandar, V., Zhao, S., Hoffie, I., Hensel, G., Rajaraman, J., Moya, Y.A.T., et al. (2023). A molecular framework for grain number determination in barley. Sci. Adv. *9*, eadd0324. https://doi.org/10.1126/sciadv.add0324.
39. Rutten, T., Thirulogachandar, V., Huang, Y., Shanmugaraj, N., Koppolu, R., Ortleb, S., Hensel, G., Kumlehn, J., Melzer, M., and Schnurbusch, T. (2024). Anatomical insights into the vascular lay-out of the barley rachis: implications for transport and spikelet connection. Ann. Bot. https://doi.org/10.1093/aob/mcae025.
40. Iyer, L.M., and Aravind, L. (2012). ALOG domains: provenance of plant homeotic and developmental regulators from the DNA-binding domain of a novel class of DIRS1-type retroposons. Biol. Direct *7*, 39. https://doi.org/10.1186/1745-6150-7-39.
41. Naramoto, S., Hata, Y., and Kyozuka, J. (2020). The origin and evolution of the ALOG proteins, members of a plant-specific transcription factor family, in land plants. J. Plant Res. *133*, 323–329. https://doi.org/10.1007/s10265-020-01171-6.
42. Naramoto, S., Jones, V.A.S., Trozzi, N., Sato, M., Toyooka, K., Shimamura, M., Ishida, S., Nishitani, K., Ishizaki, K., Nishihama, R., et al.

(2019). A conserved regulatory mechanism mediates the convergent evolution of plant shoot lateral organs. PLoS Biol. *17*, e3000560. https://doi.org/10.1371/journal.pbio.3000560.

43. Waddington, S.R., Cartwright, P.M., and Wall, P.C. (1983). A quantitative scale of spike initial and pistil development in barley and wheat. Ann. Bot. *51*, 119–130. https://doi.org/10.1093/oxfordjournals.aob.a086434.
44. Hibara, K.-I., Karim, M.R., Takada, S., Taoka, K.-I., Furutani, M., Aida, M., and Tasaka, M. (2006). Arabidopsis CUP-SHAPED COTYLEDON3 regulates postembryonic shoot meristem and organ boundary formation. Plant Cell *18*, 2946–2957. https://doi.org/10.1105/tpc.106.045716.
45. Douglas, S.J., Chuck, G., Dengler, R.E., Pelecanda, L., and Riggs, C.D. (2002). KNAT1 and ERECTA regulate inflorescence architecture in Arabidopsis. Plant Cell *14*, 547–558. https://doi.org/10.1105/tpc.010391.
46. Poursarebani, N., Trautewig, C., Melzer, M., Nussbaumer, T., Lundqvist, U., Rutten, T., Schmutzer, T., Brandt, R., Himmelbach, A., Altschmied, L., et al. (2020). COMPOSITUM 1 contributes to the architectural simplification of barley inflorescence via meristem identity signals. Nat. Commun. *11*, 5138. https://doi.org/10.1038/s41467-020-18890-y.
47. Xu, Y., Prunet, N., Gan, E.S., Wang, Y., Stewart, D., Wellmer, F., Huang, J., Yamaguchi, N., Tatsumi, Y., Kojima, M., et al. (2018). SUPERMAN regulates floral whorl boundaries through control of auxin biosynthesis. EMBO J. *37*, e97499. https://doi.org/10.15252/embj.201797499.
48. Miguel, V.N., Manavella, P.A., Chan, R.L., and Capella, M.A. (2020). The AtHB1 transcription factor controls the miR164-CUC2 regulatory node to modulate leaf development. Plant Cell Physiol. *61*, 659–670. https://doi.org/10.1093/pcp/pcz233.
49. Maier, A.T., Stehling-Sun, S., Offenburger, S.L., and Lohmann, J.U. (2011). The bZIP transcription factor PERIANTHIA: a multifunctional hub for meristem control. Front. Plant Sci. *2*, 79. https://doi.org/10.3389/fpls.2011.00079.
50. Lee, D.-Y., and An, G. (2012). Two AP2 family genes, SUPERNUMERARY BRACT (SNB) and OsINDETERMINATE SPIKELET 1 (OsIDS1), synergistically control inflorescence architecture and floral meristem establishment in rice. Plant J. *69*, 445–461. https://doi.org/10.1111/j.1365-313x.2011.04804.x.
51. Koppolu, R., Anwar, N., Sakuma, S., Tagiri, A., Lundqvist, U., Pourkheirandish, M., Rutten, T., Seiler, C., Himmelbach, A., Ariyadasa, R., et al. (2013). Six-rowed spike4 (Vrs4) controls spikelet determinacy and row-type in barley. Proc. Natl. Acad. Sci. USA *110*, 13198–13203.
52. Kumaran, M.K., Ye, D., Yang, W.-C., Griffith, M.E., Chaudhury, A.M., and Sundaresan, V. (1999). Molecular cloning of ABNORMAL FLORAL ORGANS: a gene required for flower development in Arabidopsis. Sex. Plant Reprod. *12*, 118–122.
53. Sawa, S., Watanabe, K., Goto, K., Liu, Y.G., Shibata, D., Kanaya, E., Morita, E.H., and Okada, K. (1999). FILAMENTOUS FLOWER, a meristem and organ identity gene of Arabidopsis, encodes a protein with a zinc finger and HMG-related domains. Genes Dev. *13*, 1079–1088. https://doi.org/10.1101/gad.13.9.1079.
54. Zhong, J., van Esse, G.W., Bi, X., Lan, T., Walla, A., Sang, Q., Franzen, R., and von Korff, M. (2021). INTERMEDIUM-M encodes an HvAP2L-H5 ortholog and is required for inflorescence indeterminacy and spikelet determinacy in barley. Proc. Natl. Acad. Sci. USA *118*, e2011779118. https://doi.org/10.1073/pnas.2011779118.
55. Ramsay, L., Comadran, J., Druka, A., Marshall, D.F., Thomas, W.T.B., Macaulay, M., MacKenzie, K., Simpson, C., Fuller, J., Bonar, N., et al. (2011). INTERMEDIUM-C, a modifier of lateral spikelet fertility in barley, is an ortholog of the maize domestication gene TEOSINTE BRANCHED 1. Nat. Genet. *43*, 169–172. https://doi.org/10.1038/ng.745.
56. Sun, R., Wang, S., Ma, D., Li, Y., and Liu, C. (2019). Genome-wide analysis of cotton auxin early response gene families and their roles in somatic embryogenesis. Genes *10*, 730. https://doi.org/10.3390/genes10100730.
57. Chapman, E.J., and Estelle, M. (2009). Mechanism of auxin-regulated gene expression in plants. Annu. Rev. Genet. *43*, 265–285. https://doi.org/10.1146/annurev-genet-102108-134148.
58. Leyser, O. (2018). Auxin signaling. Plant Physiol. *176*, 465–479. https://doi.org/10.1104/pp.17.00765.
59. Stortenbeker, N., and Bemer, M. (2019). The SAUR gene family: the plant's toolbox for adaptation of growth and development. J. Exp. Bot. *70*, 17–27. https://doi.org/10.1093/jxb/ery332.
60. Keuskamp, D.H., Pollmann, S., Voesenek, L.A.C.J., Peeters, A.J.M., and Pierik, R. (2010). Auxin transport through PIN-FORMED 3 (PIN3) controls shade avoidance and fitness during competition. Proc. Natl. Acad. Sci. USA *107*, 22740–22744. https://doi.org/10.1073/pnas.1013457108.
61. Kuijer, H.N.J., Shirley, N.J., Khor, S.F., Shi, J., Schwerdt, J., Zhang, D., Li, G., and Burton, R.A. (2021). Transcript profiling of MIKCc MADS-Box genes reveals conserved and novel roles in barley inflorescence development. Front. Plant Sci. *12*, 705286. https://doi.org/10.3389/fpls.2021.705286.
62. Shin, K., Lee, I., Kim, E., Park, S.K., Soh, M.-S., and Lee, S. (2019). PACLOBUTRAZOL-RESISTANCE gene family regulates floral organ growth with unequal genetic redundancy in Arabidopsis thaliana. Int. J. Mol. Sci. *20*, 869. https://doi.org/10.3390/ijms20040869.
63. Gorham, S.R., Weiner, A.I., Yamadi, M., and Krogan, N.T. (2018). HISTONE DEACETYLASE 19 and the flowering time gene FD maintain reproductive meristem identity in an age-dependent manner. J. Exp. Bot. *69*, 4757–4771. https://doi.org/10.1093/jxb/ery239.
64. Thiel, J., Koppolu, R., Trautewig, C., Hertig, C., Kale, S.M., Erbe, S., Mascher, M., Himmelbach, A., Rutten, T., Esteban, E., et al. (2021). Transcriptional landscapes of floral meristems in barley. Sci. Adv. *7*, eabf0832.
65. Sakuma, S., Golan, G., Guo, Z., Ogawa, T., Tagiri, A., Sugimoto, K., Bernhardt, N., Brassac, J., Mascher, M., Hensel, G., et al. (2019). Unleashing floret fertility in wheat through the mutation of a homeobox gene. Proc. Natl. Acad. Sci. USA *116*, 5182–5187. https://doi.org/10.1073/pnas.1815465116.
66. Liu, L., Lindsay, P.L., and Jackson, D. (2021). Next generation cereal crop yield enhancement: from knowledge of inflorescence development to practical engineering by genome editing. Int. J. Mol. Sci. *22*, 5167. https://doi.org/10.3390/ijms22105167.
67. Chen, Z., and Gallavotti, A. (2021). Improving architectural traits of maize inflorescences. Mol. Breed. *41*, 21. https://doi.org/10.1007/s11032-021-01212-5.
68. Meyer, R.S., and Purugganan, M.D. (2013). Evolution of crop species: genetics of domestication and diversification. Nat. Rev. Genet. *14*, 840–852. https://doi.org/10.1038/nrg3605.
69. Takeda, S., Matsumoto, N., and Okada, K. (2004). RABBIT EARS, encoding a SUPERMAN-like zinc finger protein, regulates petal development in Arabidopsis thaliana. Development *131*, 425–434. https://doi.org/10.1242/dev.00938.
70. Gauley, A., Pasquariello, M., Yoshikawa, G.V., Allabdullah, A.K., Hayta, S., Smedley, M.A., Dixon, L.E., and Boden, S.A. (2024). *Photoperiod-1* regulates the wheat inflorescence transcriptome to influence spikelet architecture and flowering time. Curr. Biol. Published online May 22, 2024. https://doi.org/10.1016/j.cub.2024.04.029.
71. Martin, M. (2011). Cutadapt removes adapter sequences from high-throughput sequencing reads. EMBnet. J. *17*, 10. https://doi.org/10.14806/ej.17.1.200.
72. Li, H. (2013). Aligning sequence reads, clone sequences and assembly contigs with BWA-MEM. Preprint at arXiv. https://doi.org/10.48550/arXiv.1303.3997.
73. Li, H., Handsaker, B., Wysoker, A., Fennell, T., Ruan, J., Homer, N., Marth, G., Abecasis, G., and Durbin, R.; 1000 Genome Project Data Processing Subgroup (2009). The Sequence Alignment/Map format and SAMtools. Bioinformatics *25*, 2078–2079. https://doi.org/10.1093/bioinformatics/btp352.
74. Danecek, P., Auton, A., Abecasis, G., Albers, C.A., Banks, E., Depristo, M.A., Handsaker, R.E., Lunter, G., Marth, G.T., Sherry, S.T., et al. (2011).

The variant call format and VCFtools. Bioinformatics *27*, 2156–2158. https://doi.org/10.1093/bioinformatics/btr330.

75. Pertea, M., Kim, D., Pertea, G.M., Leek, J.T., and Salzberg, S.L. (2016). Transcript-level expression analysis of RNA-seq experiments with HISAT, StringTie and Ballgown. Nat. Protoc. *11*, 1650–1667. https://doi.org/10.1038/nprot.2016.095.
76. Liao, Y., Smyth, G.K., and Shi, W. (2014). featureCounts: an efficient general purpose program for assigning sequence reads to genomic features. Bioinformatics *30*, 923–930. https://doi.org/10.1093/bioinformatics/btt656.
77. Love, M.I., Huber, W., and Anders, S. (2014). Moderated estimation of fold change and dispersion for RNA-seq data with DESeq2. Genome Biol. *15*, 550. https://doi.org/10.1186/s13059-014-0550-8.
78. Minh, B.Q., Schmidt, H.A., Chernomor, O., Schrempf, D., Woodhams, M.D., Von Haeseler, A., and Lanfear, R. (2020). IQ-TREE 2: new models and efficient methods for phylogenetic inference in the genomic era. Mol. Biol. Evol. *37*, 1530–1534. https://doi.org/10.1093/molbev/msaa015.
79. Marthe, C., Kumlehn, J., and Hensel, G. (2015). Barley (Hordeum vulgare L.) transformation using immature embryos. Methods Mol. Biol. *1223*, 71–83. https://doi.org/10.1007/978-1-4939-1695-5_6.
80. Kirby, E., and Appleyard, M. (1984). Cereal Development Guide, 2nd Edition.
81. Monat, C., Padmarasu, S., Lux, T., Wicker, T., Gundlach, H., Himmelbach, A., Ens, J., Li, C., Muehlbauer, G.J., Schulman, A.H., et al. (2019). TRITEX: chromosome-scale sequence assembly of Triticeae genomes with open-source tools. Genome Biol. *20*, 284. https://doi.org/10.1186/s13059-019-1899-5.
82. Li, H. (2011). A statistical framework for SNP calling, mutation discovery, association mapping and population genetical parameter estimation from sequencing data. Bioinformatics *27*, 2987–2993. https://doi.org/10.1093/bioinformatics/btr509.
83. Colmsee, C., Beier, S., Himmelbach, A., Schmutzer, T., Stein, N., Scholz, U., and Mascher, M. (2015). BARLEX – the Barley Draft Genome Explorer. Mol. Plant *8*, 964–966. https://doi.org/10.1016/j.molp.2015.03.009.
84. Budhagatapalli, N., Schedel, S., Gurushidze, M., Pencs, S., Hiekel, S., Rutten, T., Kusch, S., Morbitzer, R., Lahaye, T., Panstruga, R., et al. (2016). A simple test for the cleavage activity of customized endonucleases in plants. Plant Methods *12*, 18. https://doi.org/10.1186/s13007-016-0118-6.
85. Lolas, I.B., Himanen, K., Grønlund, J.T., Lynggaard, C., Houben, A., Melzer, M., Van Lijsebettens, M., and Grasser, K.D. (2010). The transcript elongation factor FACT affects Arabidopsis vegetative and reproductive development and genetically interacts with HUB1/2. Plant J. *61*, 686–697. https://doi.org/10.1111/j.1365-313x.2009.04096.x.
86. Gu, Z., Eils, R., and Schlesner, M. (2016). Complex heatmaps reveal patterns and correlations in multidimensional genomic data. Bioinformatics *32*, 2847–2849. https://doi.org/10.1093/bioinformatics/btw313.
87. Zhou, Y., Zhou, B., Pache, L., Chang, M., Khodabakhshi, A.H., Tanaseichuk, O., Benner, C., and Chanda, S.K. (2019). Metascape provides a biologist-oriented resource for the analysis of systems-level datasets. Nat. Commun. *10*, 1523. https://doi.org/10.1038/s41467-019-09234-6.
88. Letunic, I., and Bork, P. (2021). Interactive Tree Of Life (iTOL) v5: an online tool for phylogenetic tree display and annotation. Nucleic Acids Res. *49*, W293–W296. https://doi.org/10.1093/nar/gkab301.
89. Rajaraman, J., Douchkov, D., Lück, S., Hensel, G., Nowara, D., Pogoda, M., Rutten, T., Meitzel, T., Brassac, J., Höfle, C., et al. (2018). Evolutionarily conserved partial gene duplication in the Triticeae tribe of grasses confers pathogen resistance. Genome Biol. *19*, 1–18. https://doi.org/10.1186/s13059-018-1472-7.
90. Jackson, D. (1991). In situ hybridization in plants. In Molecular Plant Pathology: A Practical Approach (Oxford University Press).

STAR★METHODS

KEY RESOURCES TABLE

REAGENT or RESOURCE	SOURCE	IDENTIFIER
Bacterial and virus strains		
E. coli strain: DH5a	Widely distributed	N/A
Agrobacterium tumefaciens strain: AGL1	Widely distributed	N/A
Chemicals, peptides, and recombinant proteins		
Xylene	Roth	Cat#CN80.1
Anti-Digoxigenin-AP	Merck	Cat#11745832910
NBT-BCIP	Merck	Cat#11681451001
TRIzol	Invitrogen	Cat#15596026
Critical commercial assays		
SuperScript III One-Step RT-PCR System	Invitrogen	Cat#12574026
SYBR Green Master Mix	Thermo Fisher Scientific	Cat#A46112
PrimeSTAR GXL DNA Polymerase	Takala	Cat#R050B
T4 DNA Ligase (400.000 units/ml)	New England BioLabs	Cat#M0202L_37612
ClonExpress II One Step Cloning Kit	Vazyme	Cat#C112
Deposited data		
Raw WGS data: *flo.a*	This paper	ENA: PRJEB67397
Raw RNA-seq data: Bowman and *flo.a*	This paper	ENA: PRJEB67396
Experimental models: Organisms/strains		
Barley: cultivar Bowman	IPK	N/A
Barley: cultivar Foma	IPK	N/A
Barley: cultivar Golden Promise	IPK	N/A
Barley: *flo.a*	USDA–ARS https://npgsweb.ars-grin.gov/gringlobal/search	GSHO 2005
Barley: *flo.b*	USDA–ARS https://npgsweb.ars-grin.gov/gringlobal/search	GSHO 2128
Barley: *flo.c*	USDA–ARS https://npgsweb.ars-grin.gov/gringlobal/search	GSHO 1877
Barley: *flo-like* mutants	NGRC, NordGen https://www.nordgen.org/en/	N/A
Oligonucleotides		
See Table S5	This paper	N/A
Recombinant DNA		
pGEM-T	Widely distributed	N/A
p6i-d35S-TE9	DNA Cloning Service e.K.	N/A
P35S-EGFP	This paper	N/A
HvALOG1-p::HvALOG1:GFP	This paper	N/A
Cas9_*HvALOG1*	This paper	N/A
Software and algorithms		
Zen 2.3 blue edition	Carl Zeiss Microscopy GmbH	www.zeiss.com/microscopy/int/products/microscope-software/zen.html
Fiji	ImageJ	https://fiji.sc/
Inkscape	N/A	https://inkscape.org/
Prism	GraphPad	https://www.graphpad.com/

(*Continued on next page*)

Continued

REAGENT or RESOURCE	SOURCE	IDENTIFIER
R	R Core Team	https://www.r-project.org/
FastQC (version 0.11.9)	Babraham Bioinformatics	https://www.bioinformatics.babraham.ac.uk/projects/fastqc/
Cutadapt	Martin[71]	https://cutadapt.readthedocs.io/en/stable/
BWA-MEM version 0.7.12a	Li[72]	https://arxiv.org/abs/1303.3997
SAMtools	Li et al.[73]	http://www.htslib.org/
VCFtools	Danecek et al.[74]	https://vcftools.github.io/
Trim Galore (version 0.6.5)	Babraham Bioinformatics	https://www.bioinformatics.babraham.ac.uk/projects/trim_galore/)
HISAT2 (version 2.2.1)	Pertea et al.[75]	https://daehwankimlab.github.io/hisat2/
featureCounts (version 1.22.2)	Liao et al.[76]	https://subread.sourceforge.net/
DESeq2 (version 3.13)	Love et al.[77]	https://doi.org/10.1186/s13059-014-0550-8
Clustal Omega	EMBL-EBI	https://www.ebi.ac.uk/Tools/msa/clustalo/
IQ-tree (v2.1.3)	Minh et al.[78]	http://www.iqtree.org/
iTOL	N/A	https://itol.embl.de/itol.cgi
MUSCLE algorithm	MEGA 11	https://www.megasoftware.net/
Amira	Thermo Fischer Scientific	https://www.thermofisher.com/de/de/home/electron-microscopy/products/software-em-3d-vis/amira-software.html

RESOURCE AVAILABILITY

Lead contact

Further information and requests for resources and reagents should be directed to and will be fulfilled by the lead contact, Thorsten Schnurbusch (schnurbusch@ipk-gatersleben.de).

Materials availability

All unique and stable reagents produced in this study can be obtained from the lead contact upon completion of a Materials Transfer Agreement.

Data and code availability

- Whole genome sequencing data for Foma and *flo.a*, along with RNA-seq data for Bowman and *flo.a*, have been deposited at the European Nucleotide Archive (ENA) and are publicly accessible as of the publication date. Accession numbers can be found in the key resources table. All data reported in this study are publicly available upon the date of publication and will be shared by the lead contact upon request.
- This paper does not report original code.
- Any additional information required to reanalyze the data reported in this paper is available from the lead contact upon request.

EXPERIMENTAL MODEL AND SUBJECT DETAILS

Three *flo* (*flo.a*, GSHO 2005; *flo.b*, GSHO 2128; *flo.c,* GSHO 1877) mutants used in this study were obtained from the United States Department of Agriculture (USDA–ARS), USA. In addition, a set of nine *flo-like* mutants were obtained from Dr. Udda Lundqvist, Nordic Genetic Resources Center (NGRC, NordGen), Sweden.

For genetic analysis and preliminary mapping, one BW-NIL of *flo* mutant, namely *flo.a*, was used for the construction of a segregating population: *flo.a* was crossed with recurrent parent BW to generate F1 plants, followed by self-pollinating to form F2 population of 192 plants. Subsequently, the phenotypes were investigated, and molecular markers were designed to harvest recombinants in the F2 population to determine the linkage relationship between phenotype and genotype. For fine mapping, the recombinant plants from the F2 population were grown into the next F3 generation to form a segregating population of around 3,800 plants.

Barley plants were initially germinated in 96-well plates. Then, seedlings of two weeks were transferred to the vernalization room (4°C) for 4 weeks. The vernalized plants were transplanted into individual pots (11 cm diameter) under greenhouse conditions (20°C in day / 15 °C at night, 16h of light / 8h of dark). In addition, wild-type plants and *flo* mutants were grown in the field. After germinated in

greenhouse condition, the seedlings were transplanted in the field in the Leibniz Institute of Plant Genetics and Crop Plant Research, Gatersleben, Germany (51° 49′ 23″ N, 11° 17′ 13″ E, altitude 112 m).

For transgenic plants, the clustered regularly interspaced short palindromic repeats (CRISPR)-associated (Cas9) endonuclease-induced knock-out and green fluorescent protein (GFP)-reporter plants in cv. Golden Promise background were generated as previously described.[79] All transgenic plants were grown in the greenhouse under the conditions mentioned above.

METHOD DETAILS

Barley phenotyping

Morphological observation of spikes was performed between wild-type (Bowman) and *flo* mutants at early developing and mature stages. After the transition from vegetative to reproductive growth, the young spikes of BW and *flo* mutants were dissected and characterized in several key developing stages, including double ridge (DR), triple mound (TM), glume primordium (GP), lemma primordium (LP), stamen primordium (SP), awn primordium (AP), white anther (WA).[80] Developmental details of inflorescences in WTs and *flo* mutants were photographed using a stereomicroscope with a digital camera (Leica, MZ FLIII).

Once matured, all well-fruited spikes were harvested intact and characterized. Morphology and number of triple spikelets were compared between wild-types and *flo* mutants. Additional yield related agronomic traits investigated included: plant height, spikelet number per spike, node number per spike, spike length, grain number per spike, grain setting rate, grain length, grain width, thousand-grain weight, and grain area.

WGS and introgression identification

Genomic DNA of Foma and *flo.a* was extracted by using fresh leaves and the quality and concentration by agarose gel electrophoresis and Qubit 2.0 were determined, respectively. Subsequently, DNA was used for whole-genome sequencing (WGS) by using Illumina sequencing platform at Novogene Co., Ltd (Cambridge, UK) to harvest 150 bp paired-end reads with 10X coverage of the ~5.1 Gb barley genome. The raw reads were trimmed using Cutadapt[71] and aligned to barley reference genome of *cv.* Morex Version 2 (V2)[81] using BWA-MEM version 0.7.12a.[72] Alignment records were converted into binary alignment map (BAM) files and sorted by reference position and indexed using Samtools.[73] Variants were called between BW and *flo.a* using SAMtools/BCFtools version 1.6[82] to generate VCF files. The heterozygous SNPs were removed and homozygous SNPs were filtered with Minimum allele frequency (MAF) > 0.5 to obtain SNPs only exist between BW and *flo.a* using VCFtools.[74] Finally, the number and density of SNPs were calculated in bins of size with 100K bp with VCFtools and visualized with R. Continuous bins with high density of SNPs can be regarded as introgression from *flo.a*.

Genetic analysis and map-based cloning

The *flo.a* mutant was initially crossed with BW to generate F1 hybrids, for which genuine hybrids were identified by polymorphic molecular markers. The '*flo*' phenotype was investigated in the F2 population. A chi-square test was performed to estimate whether the ratio of observed mutant type and observed wild-type is in line with the single gene segregation (1:3).

After identifying three introgressions on chromosomes 3H (1x) and 6H (2x) in the *flo.a*, molecular markers were designed based on the previously obtained SNPs matrix by WGS, to determine the phenotype-genotype linkage relationship. Since the *Flo.a* allele has been reported previously to locate on chromosome 6H,[9,37] molecular markers on 6H were designed for initial linkage analysis. *Flo.a* was preliminarily mapped into an interval between two markers FB-74.4 and FB-115.0 on the short arm of chromosome 6H using F2 population. For high-resolution mapping within the *Flo.a* genomic interval, a large F3 segregating population was generated derived from the self-pollination of recombinants from F2 population and 3,794 individuals were used for fine mapping with newly developed CAPS and Indel markers. The sequences of all markers for mapping are listed in (Table S5). Genotyping and linkage analysis revealed that *flo.a* was associated with two molecular markers, FB74.4 and FB110.0, on the short arm of chromosome 6H, partially overlapping with the introgression from the original mutant (Figure 3A).

Inducing targeted knock-out mutations

A barley transformation platform established in IPK-Gatersleben was used to create the barley transgenic plants.[79] For inducing KO mutations in *HvALOG1* and its closest paralog on 7H (*HvALOG2*) mediated by Cas9-mediated genome editing, the coding regions of *HvALOG1* and *HvALOG2* of the two-rowed barley *cv.* Golden Promise was sequenced and used for guide RNA (gRNA) design. Two 20-bp gene-specific guide RNA sequences targeting *HvALOG1* or *HvALOG2* were selected using the online prediction tool (https://www.deskgen.com/guidebook/). The targeting specificity in the barley genome was examined using blast search (https://apex.ipk-gatersleben.de/apex/f?p=284:10::::::#HOME_LINK#).[83] The secondary structures of gRNA were predicted by RNAfold (http://rna.tbi.univie.ac.at/cgi-bin/RNAWebSuite/RNAfold.cgi) to select the most suitable target motifs. The oligonucleotides of target-specific gRNA sequences were synthesized, annealed, and ligated into the monocot-compatible intermediate vector pSH91.[84] Subsequently, the expression units for gRNA and Cas9 were subcloned into the binary vector p6i-d35S-TE9 (DNA Cloning Service e.K., Germany) by using the *SfiI* restriction sites. The two resulting constructs were used to transform *cv.* Golden Promise by inoculation of immature embryos with *Agrobacterium tumefaciens* AGL1. A total of 34 independent transgenic plants (T0) were generated and

grown under greenhouse conditions. PCR-based Sanger-sequencing was performed to detect the presence/absence of the T-DNA and the mutation sites in the target genes. The sequence of oligonucleotides and all primers for detecting transgenic plants are listed in (Table S5).

Construction of GFP reporter plants

The GFP-reporter plants were produced using a *HvALOG1* and *GFP* translational fusion construct. The *HvALOG1-p*:HvALOG1:GFP construct was created by fusing the 2,550 bp *HvALOG1* promoter, full-length (780 bp without TAG) *HvALOG1* cDNA, enhanced green fluorescent protein (eGFP) and 1,065 bp 3′ untranslated region (UTR) of *HvALOG1*, followed by cloning into the binary vector p6i-d35S-TE9 (DNA Cloning Service e.K., Germany). This vector was used to transform barley *cv.* Golden Promise using *Agrobacterium tumefaciens* AGL1. The primers used for construction are listed in (Table S5).

Scanning electron microscopy analysis

Immature spike tissues from seven stages, including DR, TM, GP, LP, SP, AP, WA as well as mature spikelets were collected from BW and *flo.a* growing in the greenhouse. The fixation, processing and photographing of samples mainly refer to published literature.[46] SEM was conducted by following a protocol established in IPK-Gatersleben.[85] Probes were examined using a Zeiss Gemini300 scanning electron microscope (Carl Zeiss Microscopy GmbH). All images were recorded digitally.

mRNA isolation and qRT-PCR

The developing spike tissues of *flo.a* and BW were collected for mRNA isolation from DR, TM, GP, LP, SP, AP, WA stages using the stereoscopic microscope.[80] Total RNA was extracted using TRIzol (Invitrogen). The total RNA was treated with DNase I (Fermentas) to remove genomic DNA contamination. The cDNA was synthesized from 2μg RNA using SuperScript III reverse transcriptase and oligo (dT) primer (Invitrogen, 18080-051). Transcript levels of target genes were measured by qRT-PCR with SYBR Green Master Mix (Thermo Fisher Scientific, A46112) under ABI Prism 7900HT sequence detection system machine (Applied Biosystems). All primers for qRT–PCR are listed in (Table S5). For each sample, qRT-PCR was performed technically three times, and each sample collection was carried out independently three times. The resulting data represented the average transcription levels, which were subsequently normalized using the barley actin gene. Significance tests were calculated by using the Student's *t*-test (two-tailed).

RNA sequencing

Immature spike samples of BW and *flo.a* plants were collected at Waddington stages W2.0 (DR), W3.0 (LP), W4.5 (AP) and W5.5 (WA).[43] Due to the '*flo*' spikelet phenotype only existing in the upper-mid portion of spike, the whole spike was transversely sectioned into two parts (upper-mid and basal) at stages W3.0, W4.5 and W5.5 under a stereoscopic microscope. A total of 15-48 spikes per sample and three biological replicates were harvested and used for RNA extraction (protocol described previously). The integrity and quantities of RNA were determined using an Agilent 2100 Bioanalyzer (Agilent Technologies). A total of 1 μg of high-integrity RNA of each sample was used for the construction of sequencing library. The total mRNA was enriched using oligo(dT) beads, followed by random fragmentation using a fragmentation buffer. Strand-specific RNA libraries were generated using TruSeq Stranded mRNA Sample Prep Kit (Illumina) according to the instructions of the manufacturer. High-throughput paired-end sequencing was conducted using a NovaSeq 6000 PE150 Platform (Illumina) at Novogene Co., Ltd (Cambridge, UK).

RNA-seq data analysis

The raw reads were assessed for quality initially using FastQC (version 0.11.9) (http://www.bioinformatics.babraham.ac.uk/projects/fastqc/), following conducted automated adapters trimming and quality control using Trim Galore (version 0.6.5) (https://www.bioinformatics.babraham.ac.uk/projects/trim_galore/) to harvest high-quality reads. Subsequently, the sequences were aligned to the barley reference genome *cv.* Morex V2[81] using HISAT2 (version 2.2.1).[75] The read counts that reflect the level of gene transcription were obtained by featureCounts (version 1.22.2).[76] The raw read counts were normalized to Transcripts Per Kilobase Million (TPM) expression levels. Differential gene expression analysis was performed using DESeq2 (version 3.13) package in R.[77] Differentially expressed genes (DEGs) were called in pairwise comparisons of each of the stages and positions. The Benjamini-Hochberg method was implemented to calculate *p-values* and adjusted *p-values* by False Discovery Rate (FDR) for the significant test. The DEGs were identified by using the threshold of adjusted *p-values* < 0.05 and log2 fold change ≥ 0.5845 or ≤ -0.5845.

The high-confidence (HC) genes in identified DEGs were used for further analysis. Heatmap for HC DEGs was produced using ComplexHeatmap package in R.[86] Cluster analysis for HC DEGs was performed using Z-scored normalized TPM by the K-medoids method with the PAM algorithm function. For GO term enrichment analysis, *Arabidopsis* closest homologs were identified by BLASTp in TAIR10 (*e-value* $< 1e-5$) using the deduced sequences of barley HC protein. The corresponding *Arabidopsis* homologs to HC DEGs from clusters 1 to 8 were applied to GO term enrichment, summarization and visualization using Metascape with the default parameters (http://metascape.org).[87]

Phylogenetic analysis

The phylogenetic analysis of ALOG proteins is based on the amino acid sequence of the ALOG domain. The domain of *HvALOG1* is first implemented in BLASTp with a cutoff *e–value* of 1e-30 in proteomes from 14 plant species including 8 monocots and 6 eudicots: *Hordeum vulgare*, *Zea mays*, *Oryza sativa*, *Sorghum bicolor*, *Triticum aestivum*, *Brachypodium distachyon*, *Setaria viridis*, *Secale*

cereale, *Gossypium raimondii*, *Glycine max*, *Arabidopsis thaliana*, *Brassica rapa*, *Populus trichocarpa*, *Solanum lycopersicum*. Subsequently, all sequences of the retrieved proteins within the ALOG family were aligned using Clustal Omega (https://www.ebi.ac.uk/Tools/msa/clustalo/). The phylogenetic analysis was constructed based on maximum likelihood (ML) criterion by using IQ-tree (v2.1.3) with the recommended parameter '-m MFP -B 1000 -bnni'.[78] Finally, the phylogenetic tree was visualized and modified by iTOL (https://itol.embl.de/itol.cgi).[88]

Phytohormone measurements

For phytohormone (auxin, CK, GAs and ABA) measurements, immature spikes at Waddington stage W2.0 (DR), W3.0 (LP), W4.5 (AP) and W5.5 (WA) were collected from BW and *flo.a* plants. The immature spikes were cross-sectioned into the upper-mid and basal parts for sampling according to the tipping point of the '*flo*' phenotype among the rachis node on the spike under a stereoscopic microscope. Each sample contains four to six biological replicates, and each replicate contains approximately 10 mg of immature sectioned spikes tissues. All collected samples were quickly frozen and stored at −80°C; the following samples were prepared and further subjected to the UPLC-MS platform (IPK-Gatersleben, Germany) for phytohormone quantification according to published literature.[38] Data from replicates of each sample were analyzed, and significance tests were calculated by two-way ANOVA.

Subcellular localization

The subcellular localization experiment was referred to published literature.[89] In brief, the full-length *HvALOG1* CDS, PCR amplified from BW spikes, was fused with eGFP to produce an HvALOG1-GFP transient expression construct based on P35S-EGFP expression vector driven by CaMV 35S promoter. Subsequently, the vector was transferred into barley leaf epidermis by microparticle bombardment. After two days of cultivation, the fluorescence signal was detected under an LSM780 confocal laser scanning microscope (Carl Zeiss MicroImaging). Primers for vector construction for subcellular localization were listed in (Table S5).

Light microscopy

Immature spikes from BW and *flo.a* were harvested and fixed with 1% glutaraldehyde and 4% formaldehyde in 50 mM phosphate buffer pH 7.0. After dehydration and embedding in Spurr resin, semithin sections (1.0 μm) were cut on a Reichert-Jung Ultracut S (Leica, Vienna, Austria) and stained with crystal violet. Digital recordings were made on a Zeiss Axiocam light microscope (Carl Zeiss, Jena, Germany) and stored as TIFF files.

3D reconstruction

For 3D reconstruction of individual nodes mature spikes from BW and *flo.a* were used. After fixation and Spurr embedding, serial sections (1 μm) were collected at 10 μm interval. After recording on a Zeiss Axio Scan Z1 slide reader (Carl Zeiss, Jena, Germany), image stacks were aligned with open-source Fiji-ImageJ2 software after which segmentation was carried out with Amira software (Thermo Fischer Scientific, Waltham, USA).

mRNA *in situ* hybridization

The immature spikes tissues of BW and *flo.a* at the DR, LP, SP, AP stages were collected under the observation of stereoscopic microscope and fixed in FAA (50% ethanol, 5% acetic acid and 3.7% formaldehyde) at 4°C, overnight. After alcohol dehydration with a series of ethanol (50, 70, 85, 95 and 100%), the samples were embedded into Paraplast Plus (Kendall, Mansfield, MA). RNA probes were developed based on gene-specific fragments (200 - 500 bp). The purified DNA product of *HvALOG1*, *HvALOG4* and *histone H4* was PCR-amplified from cDNA of BW spikes and was cloned into pGEM-T cloning vector, respectively. The PCR products were obtained by using the vector without mutations in the inserted fragment as templates and using fusion primers containing the T7 promoter sequence (5′-TAATACGACTCACTATAGGG-3') before the forward primers of sense probes or reversed primer of antisense probes to amplify. The fusion primers are listed in (Table S5). The sense and antisense probes were synthesized by using PCR products generated in the previous step with the T7 RNA polymerase (Roche), according to the manufacturer's instructions. For hybridization, 8 μm thick sections were prepared using a microtome. The following steps, including pre-treatment, hybridization, washing and coloration were conducted as previously described.[90]

QUANTIFICATION AND STATISTICAL ANALYSIS

Data was analyzed with GraphPad Prism or R. In all figures, significance was indicated with asterisks (*: $p < 0.05$; **: $p < 0.01$; ***: $p < 0:001$; ****: $p < 0.0001$).